Evaluation of H-pile Corrosion Rates for WI Bridges Located in Aggressive Subsurface Environments

Amir Poursaee, PhD, P.E., Associate Professor
Prasada Rangaraju, PhD, P.E., Professor
Ling Ding, Graduate Student

Glenn Department of Civil Engineering,
Clemson University

WisDOT ID no. 0092-16-03

May 2019

RESEARCH & LIBRARY UNIT

WISCONSIN HIGHWAY RESEARCH PROGRAM

WISCONSIN DOT
PUTTING RESEARCH TO WORK

TECHNICAL REPORT DOCUMENTATION PAGE

1. Report No. WHRP 0092-16-03	**2. Government Accession No.**	**3. Recipient's Catalog No.**
4. Title and Subtitle Evaluation of H-pile Corrosion Rates for WI Bridges Located in Aggressive Subsurface Environments		**5. Report Date** May2019 **6. Performing Organization Code**
7. Author(s) Amir Poursaee, Prasad Rangaraju, Ling Ding		**8. Performing Organization Report No.**
9. Performing Organization Name and Address Glenn Department of Civil Engineering, Lowry Hall Clemson University, Clemson, SC, 29634		**10. Work Unit No.** **11. Contract or Grant No.** 0092-16-03
12. Sponsoring Agency Name and Address Wisconsin Department of Transportation Hill Farms Building, Research & Library Unit 4822 Madison Yards Way Madison, WI, 53707		**13. Type of Report and Period Covered** Final Report December 2015 – May 2019 **14. Sponsoring Agency Code**

15. Supplementary Notes

16. Abstract

On September 25, 2013, Pier 22 for the Leo Frigo Bridge (B-05-381) near Green Bay, Wisconsin, moved vertically approximately two feet. One of the root causes of the vertical movement was the reduced structural capacity due to the loss of section of the steel H-piles that supported the pier as a result of severe corrosion. The purpose of this research was to evaluate the corrosion rate at a limited number of structures around the State of Wisconsin. Wisconsin Department of Transportation's (WisDOT) Bureau of Structures and Bureau of Technical Services has compiled a list of structures which could have similar subsurface conditions to those encountered at the Leo Frigo Bridge. The objective of this research was to evaluate the potential corrosion rates of the piles at a limited number of specific bridges and to develop guidelines for future investigation procedures for evaluating potential pile corrosion in the project design stage. The efforts here aimed to evaluate H-pile corrosion rates for Wisconsin bridges located in aggressive subsurface environments. The obtained information from the literature review, laboratory tests and field investigation b used to derive the following conclusions:

(i) The environments based on corrosion activity of the embedded steel was ranked, (ii) The best corrosion measurement technique(s) for monitoring the corrosion activity of steel in soil, by comparing the results from the gravimetric test and different electrochemical methods was determined, (iii) The remained service life of steel specimens in selected environments was evaluated and estimated, (iv) Different corrosion mechanisms (galvanic vs. localized or combined) were compared and the significance of each mechanism in corrosion of the H-pile in different soil environments was determined, and (v) A predictive model based on neural network was developed. Through this project, the design assumptions related to the corrosion was evaluated and confirmed. Advanced corrosion monitoring program was used during this work which enabled WisDOT to overcome some current difficulties in estimating the accurate corrosion rate of the H-piles in corrosive environments. The products of the proposed research project were the correlation between subsurface environments and the corrosion activity of the H-piles throughout the State of Wisconsin. The project reports included recommendations that will be used by WisDOT personnel as the basis for a comprehensive corrosion policy in design and installation of bridges with H-pile foundations.

17. Key Words Steel; Soil; Corrosion; Corrosion Tests; H-pile	**18. Distribution Statement** No restrictions. This document is available through the National Technical Information Service. 5285 Port Royal Road Springfield, VA 22161

19. Security Classif. (of this report) Unclassified	**20. Security Classif. (of this page)** Unclassified	**21. No. of Pages** 130	**22. Price**

Form DOT F 1700.7 (8-72) Reproduction of completed page authorized

DISCLAIMER

This research was funded through the Wisconsin Highway Research Program by the Wisconsin Department of Transportation and the Federal Highway Administration under Project 0092-16-03. The contents of this report reflect the views of the authors who are responsible for the facts and accuracy of the data presented herein. The contents do not necessarily reflect the official views of the Wisconsin Department of Transportation or the Federal Highway Administration at the time of publication.

This document is disseminated under the sponsorship of the Department of Transportation in the interest of information exchange. The United States Government assumes no liability for its contents or use thereof. This report does not constitute a standard, specification or regulation.

The United States Government does not endorse products or manufacturers. Trade and manufacturers' names appear in this report only because they are considered essential to the object of the document.

EXECUTIVE SUMMARY

This investigation aimed to study the corrosion performance of carbon steel in different soils, collected from the state of Wisconsin. Carbon steel specimens (as-received), as well as steel embed in mortar (steel-mortar) specimens to simulate the realistic H-pile design in bridges, were used in this investigation. Both as-received steel and steel-mortar specimens were embedded in as-received soils, with different physiochemical properties, i.e. pH, moisture content, resistivity, chloride content, sulfate and sulfite contents, and the mean total organic carbon concentration, for more than one year. Both specimen types were also embedded in the same as-received soils, but with increased chloride content (i.e. increased to 3% by weight of as-received soils) for more than one year. In addition, the surface of three identical as-received specimens were modified using sandblasting method for 5 minutes. These specimens were embedded in one of the collected soils. Different electrochemical measurements were conducted on the specimens to evaluate the corrosion activity of the steel in these soils.

The results showed a comparable corrosion activity of the steel-mortar specimens in all soils compared to the as-received specimens in the same soil both with and without chlorides, except for soils collected from Wausau. No correlation between the available physiochemical data of the soils and the extent of corrosion in steel specimens was observed. No information of the type and population of the bacteria in the collected soils was available. Perhaps, this information could explain the observed results. In all cases, there was a galvanic current flowing between specimens in chloride-free and chloride contaminated soils. In addition, corrosion potential values of all specimens remained relatively stable both before and after addition of chlorides, suggesting that only measuring the corrosion potential may not be an efficient method to monitor the change of corrosion behavior of steel in soil. The results of electrochemical experiments also showed significant improvement in corrosion resistance of sandblasted specimens compared to the as-received specimens.

Contents

CHAPTER 1: INTRODUCTION

1.1. Problem Statement

On September 25, 2013, Pier 22 of the Leo Frigo Bridge near Green Bay, Wisconsin, moved vertically downward approximately 2 feet. This vertical movement reduced structural capacity due to the loss of the section of the steel H-piles that supported the pier [1]. The main reason of such movement was attributed to the severe corrosion of the pile [1]. To understand the corrosion activity of the steel in similar situation and to provide framework for service life prediction of such structures, soil samples were collected from different regions of the state of Wisconsin. The laboratory corrosion measurements were conducted on the steel specimens with similar chemical composition used to make the steel piles (according to ASTM A572-50 [2]) in the collected soils samples. In addition, since concrete is usually cast over the steel pile, laboratory specimens containing steel embedded in mortar, to simulate real field condition, were prepared and their corrosion activities were examined in the laboratory. Besides, the surface of as-received steel was sandblasted for 5 minutes and their corrosion activity in one of the soils was compared to that of the as-received steel specimens in the same soil. The potential for the galvanic corrosion between specimens in as-received soils and soils with elevated chloride content was also evaluated.

1.2. Objective and scope

The objective of this work is to evaluate the corrosion activity of the steel used in the H-piles in soil samples collected from locations with different physicochemical parameters as well as to develop guidelines for future investigation procedures for evaluating potential pile corrosion in the project design stage. Steel specimens with the same composition used in the H-piles were used in

this investigation. To simulate the cast concrete over the steel pile, steel-mortar specimens were prepared and used in this study along with the as-received steel specimens.

This study aims to investigate the following:

1. Corrosion activity of as-received steel and steel-mortar specimens in as-received soil samples.
2. Corrosion activity of as-received steel and steel-mortar specimens in soil samples with elevated chloride content.
3. The galvanic effect between as-received steel specimens in as-received soils and soils with elevated chloride content.
4. The impact of connecting the old steel with new steel on the corrosion activity of steel to simulate the corrosion of the repairs structures.
5. The impact of the sandblasting on the corrosion activity of steel in soil.
6. The impact of temperature on the corrosion activity of steel in soil.

To understand the corrosion activity of the steel in similar situation and to provide framework for service life prediction of such structures, soil samples were collected from nine locations of different regions of the state of Wisconsin. The laboratory corrosion measurements were conducted on the steel specimens with similar chemical composition used to make the steel piles according to ASTM A572-50 [2] in the collected soils samples. In the field, concrete is usually cast over the steel pile. To simulate this scenario, laboratory specimens containing steel embedded in mortar were prepared and their corrosion activities were examined in the laboratory. Ding and Poursaee reported the improvement in corrosion resistance of the sandblasted steel bars in concrete

pore solution [3]. Nevertheless, no study was conducted on the impact of sandblasting of steel on its corrosion behavior in soil. Thus, the surfaces of as-received steel specimens were sandblasted for 5 minutes and their corrosion activities in one of the soils were compared to those for the as-received steel specimens in the same soil. To study the impact of the chloride content of the soil on the corrosion of steel, the chloride content of the as-received soils was also increased to 3% by weight of soil and the corrosion of the steel specimens was investigated on these soils as well. The potential for the galvanic corrosion between specimens in as-received soils and soils with elevated chloride content was also evaluated.

CHAPTER 2: BACKGROUND AND LITERATURE REVIEW

2.1. Background

Steel H-piles are widely used in bridge structures to resist vertical and lateral loads. Steel H-pile is manufactured from a variety of materials including carbon steel. While carbon steel is susceptible to corrosion, it is widely used due to its low cost and high strength. However, corrosion of the steel piles is often of concern [1, 4-7]. The factors that influence corrosion in soil are numerous such as soil type, moisture content, the position of the water table, soil resistivity, soluble ion content, soil pH, oxidation-reduction potential and the role of micro-organisms in the soil [8].

The most recent severe steel pile corrosion was observed in Pier 22 for the Leo Frigo Bridge (B-05-381) near Green Bay, Wisconsin. On September 25, 2013, Pier 22 for the Leo Frigo Bridge moved vertically downward approximately 2 feet. This vertical movement reduced structural capacity due to the loss of the section of the steel H-piles that supported the pier [1]. The main reason of such movement was attributed to the severe corrosion of the pile in that location [1]. The investigation determined that several unusual factors changed the environment that led to the severe corrosion of the steel pile foundation supporting Pier 22. The first factor was the presence of industrial porous fly ash fill in the upper layer of soil in contact with the piles and the second factor was that the water and soils surrounding the pile sections embedded in the fly ash fill contained high concentrations of chloride ions. The porous fly ash contained high levels of sulfates, was frequently moist along sections of the piles, and was porous enough to permit relatively free passage of oxygen to the surface of the piles. The combination of these factors caused rapid corrosion of sections of the embedded piles, which led to crushing/buckling of the most heavily deteriorated sections of pile. Significant loss in the thickness and width of the pile

flanges was observed around and within the collapsed region of each pile. The most significant corrosion damage and greatest section loss was reported in the region that was 1 to 2-1/2 feet above and below the failed region. Pitting corrosion was also observed, specifically in the vicinity of the failed region.

2. 2. Literature Review

2.2.1. Corrosion of Metals

Corrosion in metals is caused by the flow of electrons from one metal to another or from one location to another on the surface of the same piece of metal [9]. A corrosion cell must exist in order for corrosion to take place. The formation of corrosion cell requires the presence of an anode and a cathode, an electrical connection between the anode and the cathode, and an electrolyte. Once these conditions are met, an electric current flows and metal is consumed at the anode [10].

The potential difference between the anode and the cathode results in the migration of electrons and/or ions from the anode to the cathode along the connection between the anode and cathode while current flows from cathode to anode [11]. At the anode, electrons are lost leaving positively charged atoms combine with negatively charged ions. For example, When the anode is iron, the corrosion reaction at the presence of water and oxygen are [12]:

Anode reaction: $Fe^{2+} + 2e^{-} \rightarrow Fe$ eq. 2.1

Cathode reaction: $O_2 + 2H_2O + 4e^{-} \rightarrow 4OH^{-}$ eq. 2.2

The mass loss of the metal can be related to the current flow using the Faradays' law [13] and it is directly proportional to the current flow. Thus, the severity of corrosion is directly related to the amount of current flow.

2.2.2. Corrosion of Steel in Soil

2.2.2.1. Soil Properties

Corrosion is one of the leading causes of failures of buried or embedded steel elements in soils such as bridges, pipelines and tunnels in the United States and worldwide [14]. Corrosion of buried metallic structures in soils is also a great issue for safety and economy concern in various industrial applications, e.g. oil/gas, water, sewerage distribution systems [15]. The severe corrosion of one of the steel H-piles near pile cap due to corrosive soil caused one portion of the Leo Frigo Bridge, moving vertically downward 2 feet on Sep. 2013, ultimately leading to total cost of over $20 million [4].

Soil can be considered as a heterogeneous system of pores with colloidal characteristics. The space between the soil particles can be filled with water or gas [16]. The corrosive nature of the soil can be considered as the capacity of this environment to produce and to develop the corrosion on a metal, particularly steel [17]. The study of the soil as a corrosive environment is necessary due to the large number of buried infrastructure facilities, such as pipelines, tanks, and H-piles, as their deterioration can represent a significant economic and environmental problem through the years. Nevertheless, the soil, when compared with the other environments such as atmosphere or seawater, is difficult to be classified for potential corrosivity due to its complexity [18]. Acidification, salinity, organic and nutrient depletion, compaction, chemical contamination,

landslides, and erosion are all forms of soil degradation that can result from inappropriate land use practices and may lead to a premature corrosion of the embedded steel structure in the soil [19]. Corrosion of the steel in soil is governed by the principles of electrochemistry [20]. In low-resistivity soils with different physicochemical properties, such as composition and different moisture content, formation of the macro-cells is possible. Sharp changes in oxygen concentration in the soil along the surface of the buried metal structures may lead to different electrical potential, which produces current. The amount of current and its distribution over the surface of the metal depend on the resistivity of the soil and its polarization characteristics. The latter are determined by the degree of oxygen penetration of the soil, chloride and moisture content, granulation, and other physicochemical properties of the soil [21].

Soils are classified according to their grain size distribution. Commonly used soils, such as clay, silt and sand, are named because of the size range of their inorganic content. Sand is classified as fine (0.02-0.2 mm) and coarse (0.20-2.00 mm). Silt particle size range from 0.002 to 0.02 mm, and clay particles have diameter of <0.002 mm down to colloidal matter. Many soil properties are governed by the particle size variation. Other terms commonly used for soil classification include clay loam, loamy sand, sandy clay, silt loam, silty clay loam, sandy loam and gravel. Clay soil is very plastic by nature; it becomes sticky and impervious when saturated with water. It has more packed particles and less pore capacity for moisture and oxygen diffusion compared to the other types of soils, meaning it has poor drainage and aeration. Sand and gravel have more drainage and aeration.

In relation to the physical properties of soil, volume shrinkage is the tendency of the soil to start cracking on drying and they swell when wet. When clay/silt soil dries, it forms cracks that allow diffusion of oxygen to the pile and hence the susceptibility of a buried pile to corrosion increase. Because of the poor drainage in clay and silt, the capillary pores of these soils hold a considerable amount of water.

2.2.2.2. Consequences of Pile Corrosion

Buried steel structures, such as H-piles frequently suffer from corrosion due to their direct contact with corrosive soils, resulting in high maintenance cost and even leading to catastrophic failures in some cases [22]. The corrosion of steel piles results in reduced cross-sectional area of the pile and therefore decreased axial and lateral capacity. Resistivity and acidity are two parameters widely accepted for characterizing the soil corrosively, but they do not often correlate directly to the soil corrosivity or corrosion rate of the buried steels [23-25].

Decker et al. reported that a section loss of 25% is considered serious for a pile [26]. However, Trungesvik concluded that loss in pile capacity due to corrosion may be greater than generally assumed from the loss of section area [27]. In his work, a 25% reduction in strength was reported when a corroded specimen having a section loss of 13.6%.

2.2.2.3. Factors Influencing Steel Corrosion in Soils

Although various parameters on metallic corrosion in soils have been widely studied, such as electrical resistivity, pH, water content, redox potential, ionic species, salinity, microbial activities, soil texture, porosity and other physical factors [15, 28-30], some soil properties affecting

corrosion are still not fully understood due to the complexity of the soil medium. It has been established that corrosion of ferrous materials in soils depends primarily on the soil properties rather than the kind of ferrous material [31]. Generally, soils with high resistivity, high dissolved salt and high acidity are more aggressive towards metallic materials.

Several environmental conditions may act individually or in complex relationships to influence the corrosion rates of the buried steels. Many of these variables are highly dependent upon each other and the properties of the buried steels. Robinson defined many physical and chemical characteristics that can determine the soil corrosivity as oxygen concentration, presence of sulfate and sulfide ions, resistivity, total acidity, redox potential and others [32]. In agreement with the parameters cited above, Fitzgerald studied how the corrosivity of the soil is influenced by oxygen content, dissolved salts, pH, elements that form acids, concentration of chloride, sulfide and sulfate, resistivity, total acidity, redox potential and others, depending on specific application [33]. In addition, dissimilar metals in contact with each other, different soils in contact with the structure, different aeration, steel embedded in concrete and soil and connection between old and new steel pieces are the other factors influencing the corrosion behavior of the buried steel.

Resistivity

Resistivity, the reciprocal of conductivity, indicates the ability of an environment to carry corrosion currents. A soil's resistance (R) to the passage of electricity is the property of the soil that is an indicator of the severity of the corrosion measured in ohm-cm, resistivity can vary from 30 ohm-cm in sea water to in excess of 100,000 ohm-cm in dry sand or gravel. The AWWA (American Water Works Association) formula considers less than 700 ohm-cm to be severely

corrosive, while the steel-line industry consider anything less than 1000 ohm-cm to be “very severely corrosive” [28]. Resistivity is a function of the soil moisture and the concentration of current-carrying solution ions.

In general, the potential for metallic corrosion was thought to be more severe in moist fine-grained soils with low resistivity (<1,000 – 3,000 Ω cm) and extreme pH (<5 or >10.5) compared to other conditions [34, 35]. Table 2.1 summarizes the soil corrosivity based on soil resistivity.

Table 2.1. Corrosion severity ratings based on soil resistivity [34, 35]

Soil resistivity (Ω.cm)	Corrosivity rating
>20,000	Essentially noncorrosive
10,000 – 20,000	Mildly corrosive
5,000 – 10,000	Moderately corrosive
3,000 – 5,000	Corrosive
1,000 – 3,000	Highly corrosive
< 1,000	Extremely corrosive

pH

pH is the measure of the soil’s alkalinity or acidity, which is the logarithm of the reciprocal of hydrogen concentration. pH measurements may be useful in identifying unusual soil conditions but in most cases are only significant in distinguishing between otherwise similar soils. ASTM Test method for pH of soils for use in corrosion testing (G 51-77) indicates that soil pH should be measured in situ or immediately after a sample is removed from the field. The pH of the soil was considered as the factor most affecting underground corrosion since it was discovered. However, previous studies showed the otherwise. Penhale buried steel plates in 33 different soils for 20 years [36]. For each soil, both the pH and total acidity were measured, and no correlation was found between total acidity and corrosion rate. Rajani and Maker examined the corrosion rates of

cast iron pipes obtained under various pH conditions of pipes, working on an American Water Works Association-funded project on the methodology for estimating remaining service life [37]. Based on their data, no correlation was observed between the pH and the pitting rates. Doyle et al. compared the results of pH testing with the corrosion rates of samples from 98 sites in Ontario, Canada, and found no correlation (R^2=0.04) between pH and corrosion rates [38]. The pH has little relationship with the corrosion rate and the pH alone is a poor indicator of corrosion in buried conditions.

Chlorides

Elias and Christopher identified high concentrations of sulfates (>200 pm) and chlorides (>100 ppm) as indicatives of corrosive soil in Federal Highway Administration (FHWA) guidelines for mechanically stabilized earth (MSE) wall fill [39]. Chloride ions are generally harmful, as they participate directly in anodic dissolution reactions of metals. Also, their presence tends to decrease soil resistivity. Chlorides may occur naturally in soils as a result of brackish groundwater and historical geological sea beds. Chlorides may also come from external sources such as de-icing agents applied to road surfaces [35].

Sulfides/Sulfates

Most soils will show at least a trace of sulfides and/or sulfates, and this only may be significant in conjunction with the relevant redox potential (< + 100 mV). Sulfate levels are of more significant where concrete structures are concerned [40].

Chemical Composition of Soil

Chemical composition plays a key role in understanding how a soil influences the corrosion of buried steel. The chemical compositions of soil usually include NaCl, $CaCl_2$, $MgCl_2$, KCl, Na_2SO_4, $NaHCO_3$, and $NaNO_3$. The chemical elements that are responsible for causing corrosion are sodium, potassium, calcium and magnesium, and others are acid-forming elements, such as carbonates, bicarbonates.

Moisture Content

The moisture content of soils plays a major role in the corrosion of buried ferrous metals until a limit is reached, beyond which a decline in corrosion rates takes place. Several researchers have investigated the effect of moisture content on the corrosion of buried ferrous metals. For example, Gupta and Gupta [41] performed a series of laboratory tests on steel specimens exposed in soils taken from three locations in India. The soil types of the three sites used in these tests were sandy, sandy loam and loamy. Mild steel test specimens 50 mm × 25 mm × 1.6 mm were burnished with emery cloth, decreased with toluene and weighed. All the three soils were oven-dried at 105 °C before the test. After 6 months, the metal coupons were taken out, cleaned and weighed for mass loss measurement. In another study related to the corrosion of pipes in soils, Noor and Al-Moubaraki examined the effect of moisture content on the corrosion behavior of X60 steel in soils of different cities in Saudi Arabia at ambient temperature (29 ± 1°C) [42]. The corrosion rate of X60 steel in each soil was found to increase with increasing soil moisture content up to a maximum value of 10% and then decreased with further increase in moisture content.

Bacteria in Soil

Microbiologically Influenced Corrosion (MIC) is defined as the change in the corrosion behavior of material/metal in the presence of micro-organisms [43-45]. Bacteria are attached to the metal surface and form biofilm [43], which degrades the metal surface by changing its physical and chemical characteristics due to the biochemical activities associated with their metabolism, growth and reproduction [46]. MIC is an electrochemical corrosion influenced by the presence/action of biological agents such as, but not limited to, bacteria. One of the key elements of MIC is sulfate-reducing bacteria (SRB). SRB are anaerobic bacteria that can be found in oxygen-deficient saturated soils, with a pH from 6–8, containing sulfate ions, organic compounds and minerals, and they grow in soils at a temperature of 20–30 °C. SRB are a diverse group of heterotrophic and mixotrophic bacteria [47], they are anaerobic; in other words, they do not require oxygen for growth and activity, so as an alternative to oxygen, these bacteria use sulfate with consequent production of sulfide [48].

Perhaps, the key element of understanding how SRB can contribute to corrosion will be understanding the concept of “mixed bacterial communities” or “biofilms”. A manifestation of biofilms can be seen as “tubercles” on the surface of metallic surfaces, resulting in localized corrosion [49]. Studies showed that on metallic surfaces over time, SRB number on these surfaces increases [50], indicating that a biofilm is formed. Industrial cases where MIC is a problem are usually characterized by lack of single-type cultures-alternatively pure cultures-of one type of bacterium. Actually, even the term “micro-organism” itself refers to a wide range containing bacteria, cyanobacteria, algae, lichens and fungi [51, 52].

SRB, abundant in soil environments and easily cultured and detected and are known as one of the key microbes in the MIC process [53]. During the metabolic process, sulfate is reduced to sulfide. These biogenic sulfides react with hydrogen ions produced by metabolic activities or by cathodic reaction of the corrosion process to form hydrogen sulfide (H_2S). In classical MIC theory, SRB accelerate the removal of cathodic hydrogen by the action of their hydrogenase enzyme, which decreases cathodic overpotential and increases the corrosion rate (cathodic depolarization theory; CDT) [54]. Biogenic sulfides (or H_2S) further react with dissolved iron to form FeS film on the metal substrate [55, 56]. Iron sulfides have relatively good electric conductivity, noble electrode potential, and low hydrogen evolution overpotential. Therefore, galvanic coupling between the FeS film and nearby metal substrate is set and the corrosion is accelerated. This FeS film is not permanently cathodic toward mild steel [57]. The action of SRB is required to maintain the electrochemical activity of FeS. In soil environment, the maximum corrosion rate of steel and iron by the action of SRB is reported to be 0.7 mm/y to 7.4 mm/y [58].

2. 2. 3. Generalized Regression Neural Network (GRNN) Method for Corrosion Modeling of Steel Embedded in Soil

Several modeling approaches and methodologies were used for the prediction of corrosion of steel in different scenarios such as the multiple regression technique [59-62], support vector regression [63-65]; the fuzzy-set-based technique [65-69]; and neural network modeling [70-73]. Some of the above-mentioned models (i.e. multiple regression technique) have been shown to be effective only in very restrictive environments and are limited to capture the corrosion activity with limited variables. In addition, none of these studies has been applied to study the corrosion of steels in

soil environment. Among these methods, neural network methodology seems cable of modeling the corrosion process of steel in such an environment.

Neural networks are computational systems whose architecture and operation are inspired by people's knowledge about biological neural cells (neurons) in the human brain [74]. Neural networks have been used as promising tools in corrosion research [70, 71, 75-77]. These systems are suitable for the approximation of relations among non-structured data with a high degree of nonlinearity and incomplete data. Neural networks are particularly suitable for modeling the complex systems due to their capability of learning, adapting and generalization from measured data [78, 79].

Rosen and Silverman used the neural network technique on the data from potentiodynamic polarization scans to identify if crevice, pitting and general corrosion are concerns [80]. Trasatti and Mazza successfully predicted the crevice corrosion of stainless steel and related alloys in a near neutral chloride contaminated environment using a neural network [81]. This technique was also used to describe the risk of stress corrosion cracking (SCC) as a function of temperature, chloride concentration and oxygen content [82].

Establishing a predictive model from the measured corrosion data collected from a soil can be hardly solved by classic methods of statistic data evaluation (e.g. regression analysis). Nevertheless, as far as the PIs are concerned no study was carried out to model corrosion of steel in a soil environment using a neural network. Here, the development of a Generalized Regression Neural Network (GRNN) based model for the modeling and prediction of the corrosion current

densities and corrosion potential of carbon steel embedded in the limited number of soils with different physicochemical parameters, including pH, moisture content, resistivity, chloride, sulfate, sulfite, and mean total organic carbon concentrations in soils. There are other factors that can potentially lead to the corrosion of steel in soil environments (e.g. oxygen level), which are not considered in this study. It should be emphasized that this study was focused on initiation and development of a preliminary neural network-based model and the data used to develop the model were obtained from nine soil samples. Authors are currently working on using data from National Bureau of Standards (NBS) to improve their model and the result will be submitted for publication in the near future.

2.2.3.1. Theory

System identification is a methodology used for building mathematical models of dynamic systems from measurements of the system inputs and outputs [83]**.** The applications of system identification include any system where the inputs and outputs can be measured. This includes industrial processes, control systems, economic data, biology and the life sciences, medicine, social systems and many more [84]. Specht proposed generalized regression neural network (GRNN), a procedure that used neural networks for identification and control of nonlinear systems and involved one-pass learning [85]. GRNN is basically a neural network-based function approximation or function estimation algorithm which predicts the output of given input data. Any neural network method principally needs training data, which contain input-output, to train itself. By training the network with the training data set, the network can then predict the output/results of feeding new test data set. GRNN falls into the category of probabilistic neural networks. The use of a probabilistic neural network is especially advantageous because the network “learns” in

one pass through the data and can generalize from examples as soon as they are stored [85]. In other word, the network is able to converge to the underlying function of the data with only few training samples available. In GRNN approach, the regression of a dependent variable y on an independent x estimates the most probable value for y, if a training set is available. The regression method produces the estimated value of y which minimizes the mean-squared error.

The data available from measurements of an operating system is generally never enough for a backpropagation neural network [85]. Therefore, the use of GRNN is especially advantageous due to its ability to predict results with only few training samples available and the additional knowledge needed to get the fit in a satisfying way is relatively small.

In GRNN, the weighted average of the outputs of training dataset is used to estimate the output. The weight is calculated using the Euclidean distance between the training data and test data [85]. The probability density function used in GRNN is the normal distribution and stands on the following equation:

$$\hat{Y}(X) = \frac{\sum_{i=1}^{n} Y_i \exp(-\frac{D_i^2}{2\sigma^2})}{\sum_{i=1}^{n} \exp(-\frac{D_i^2}{2\sigma^2})} \qquad \text{eq. 2.3}$$

where,

$$D_i^2 = (X - X_i)^T (X - X_i) \qquad \text{eq. 2.4}$$

X is the input sample, X_i is the training sample, Y_i is the output of the input sample X_i, D_i^2 is the Euclidean distance from X, $\exp(-\frac{D_i^2}{2\sigma^2})$ is the activation function, and T is the matrix transpose. The contribution of the training sample is determined by the activation function. The Euclidean distance between the training sample and the point of prediction, is used as a measure of how well each training sample can represent the position of the prediction, X. If the Euclidean distance between the training sample and the point of prediction is small, the activation function becomes relatively large value, and if it is a large value, the activation function becomes relatively small value; therefore, the contribution of the remained training samples to the prediction is relatively small. If the Euclidean function is zero, the activation function becomes one and the point of evaluation is represented as the best by this training sample. σ is spread constant. When σ is large, the estimated density is forced to become smooth and it becomes a multivariate Gaussian. On the other hand, a smaller value of σ allows the estimated density to assume non-Gaussian shapes [85]. Spread constant should be adjusted by training process to minimize the error.

The objective of the training procedure is to determine the optimum value of the spread constant (σ). The best approach is finding where the mean square error (MSE) is minimum. MSE measures the performance of the network according to the equation 2.5:

$$MSE = \frac{1}{n}\sum_{i=1}^{i=n}[(Y_{GRNN})_i - (Y_{exp})_i]^2 \qquad \text{eq. 2.5}$$

where n is the number of data points, $(Y_{GRNN})_i$ is the GRNN prediction and $(Y_{exp})_i$ is the experimentally measured data. For this purpose, the input data should be divided into two sets of data: (i) training dataset and (ii) testing dataset. Then, the GRNN should be applied on the second

set (testing) based on the first set (training) and the MSE for different spread constants should be calculated. The corresponding value of σ to the minimum MSE should be determined and used in the rest of the modeling steps.

To evaluate the test results, the multiple correlation coefficient, R^2, and the mean absolute percentage error, MAPE, can be used:

$$R^2 = \frac{\sum_{i=1}^{n}(\hat{y}_i - \bar{y})^2}{\sum_{i=1}^{n}(y_i - \bar{y})^2} \quad \text{eq. 2.6}$$

$$\text{MAPE} = \frac{1}{n}\sum_{i=1}^{n}\left|\frac{\hat{y}_i - y_i}{y_i}\right| \quad \text{eq. 2.7}$$

where n denotes the number of test samples, y_i represents the ith experimentally measured value, $\hat{y}_i$ is the predicted value for the ith test data, and $\bar{y}$ is the mean measured value for all test data.

2.2.4. The Influence of the Sandblasting as a Surface Mechanical Attrition Treatment on the Electrochemical Behavior of Carbon Steel in Soil

Studies showed that alteration of the surface structure of a metal can change the mechanical properties as well as corrosion behavior of metals [86-91]. In general, the surface mechanical attrition treatment (SMAT) technique modifies the surface structure of a metal by applying severe plastic deformation through impacting milling balls or hard particles onto the specimen's surface repeatedly [86, 92-99]. Sandblasting [92, 100-102], shot peening [93, 94, 103-106] are the typical SMATs which were successfully used.

The SMAT is an effective method of inducing localized plastic deformation that results in grain refinement down to the nanometer scale without changing the chemical composition of the materials [95, 97, 107-110]. It was shown that the severe plastic deformation induced by the SMAT significantly influences the corrosion resistance of a variety of metallic materials [111-118].

Sandblasting, as a SMAT method, was used for different applications such as enhancing the surface strength [119], alteration of the modification of the surface [120], and cleaning the surface of the metal [121]. While sandblasting cleans the surface and removes the oxide layer from the surface, it also creates a local plastic deformation and grain modification on the surface [92, 122] which may lead to a compressive residual stress beneath the surface layer [102]. A study by Wang and Li showed formation of a nano-crystalline layer on the surface of the sandblasted 304 stainless steel [123]. This layer decreased the corrosion resistance of the sandblasted specimens significantly compared to the as-received specimens in a 3.5% NaCl solution. On the other hand, an investigation by Hou et al. indicated that sandblasting increased the corrosion resistance of carbon steel in an alkaline environment [124]. Ding and Poursaee also reported the significant improvement in corrosion resistance of the sandblasted specimens in an alkaline environment which was proportional to the increase in the sandblasting time. They hypothesized that the formation of calcium-rich layer combined with the enhanced passive layer on the sandblasted specimens were the reasons for the improvement [3].

CHAPTER 3: MATERIALS AND EXPERIMENTAL PROCEDURES

3.1. Steel Specimens

As-received specimens were prepared from carbon steel, satisfying ASTM A572-50, with the chemical composition given in Table 3.1.

Table 3.1. Chemical composition (%) the steel specimens

C	Si	Mn	P	S	V	Ni	Co
0.23	0.4	1.35	0.04	0.05	0.06	0.015	0.05

As-received specimens with a length of 101.6 mm (4 in.) and width of 25.4 mm (1 in) were cut and copper wire was spot welded to one end for electrical connection. To prevent extraneous effects, 25.4 mm (1 in.) of one end of each specimen with the wire connection was coated with epoxy, as shown in Figure 1(a).

Steel-mortar specimens with a length of 127 mm (steel 76.2 mm (3 in.) and mortar 50.8 mm (2 in.)) as shown in Figure 3.1 (b) were also prepared. The mortar section comprised Type I Portland cement with w/c of 0.45, and 2.5 sand/cement ratio with a maximum aggregate size of 2.36 mm. For each steel-mortar specimen, first mortar was cast as 50.8 mm (2 in.) cubes, then the steel specimen was vertically embedded into the fresh mortar with the length of 25.4 mm (1 in.). Steel-mortar specimens were wet cured for 48 hours and demolded and kept in water for 7 days before being embedded in the soil for electrochemical measurements.

The surface of as-received specimens was treated by particle with an approximately 750 µm diameter under 350 kPa of air pressure. The specimens were sandblasted for 5 minutes. Then 25.4 mm (1 in.) of one end of each specimen with the wire connection was coated with epoxy.

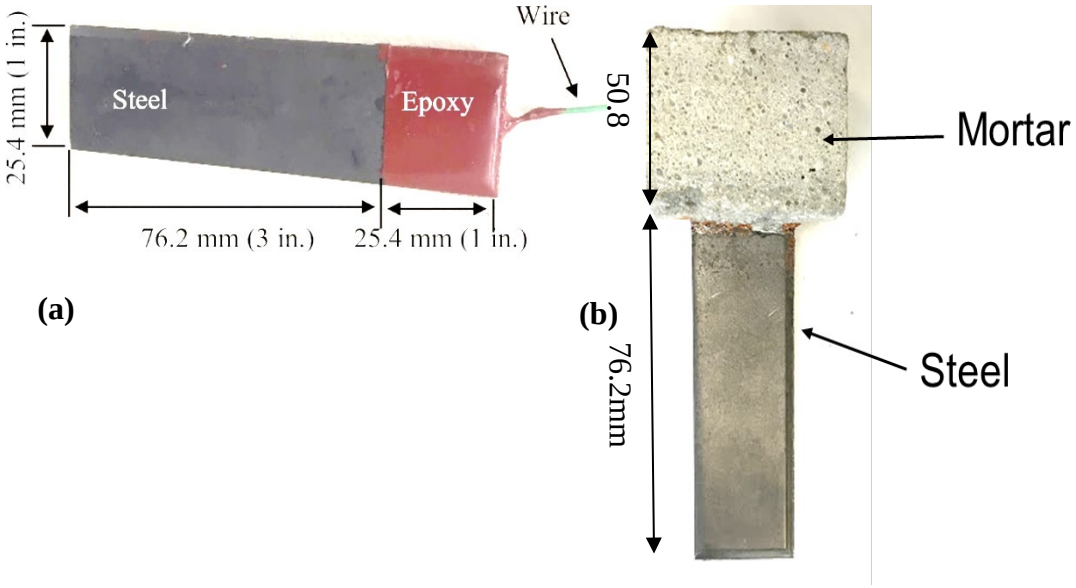

Figure 3.1. One of the (a) as-received steel specimens and (b) steel-mortar specimens.

3.2. Soil Samples

Soil samples were collected from different locations in the state of Wisconsin, as shown in Figure 3.2. Figure 3.3 shows the pictures of the locations. The physicochemical parameters of the collected soil samples were measured as followings: moisture content according to ASTM D2974-87 [125], pH by using EPA 9054 [126], soil resistivity according to EPA 120.1 [127], chloride and sulfate contents following EPA 300.0 [128], and the total organic carbon using EPA 9060 [129]. Table 3.2 shows the physicochemical parameters of 9 soil samples in group one. Two group of the soils were used in this study. The measurement cells in group one was prepared with the as-received soils, while the chloride was added and its content in the soils was adjusted to 3% by weight of the soil in group two.

Figure 3.2. Locations of the collected soils

Table 3.2. Physicochemical parameters of 9 soil samples

Location	Sample ID	Classification	Moisture Content (%)	pH	Resistivity (ohms-cm)	Chloride (w%)	Sulfate (mg/kg)	Sulfide (mg/L)	MTOC* (mg/kg)
Milwaukee	1	Silt clay	22.3	7.80	34300	0.007	33.6	<20.0	25200
	2	Silt clay	22.1	7.80	27700	0.006	34.7	<20.0	8055
Madison	3	Clay	66.9	7.0	1000	0.727	144.0	<20.0	262000
	4	Clay	37.7	6.80	2000	0.210	<31.9	<20.0	31700
	5	Clay	57.9	7.0	1200	0.582	219.0	54.7	37400
	6	Silt clay	32.1	7.90	3200	0.143	<29.2	<20.0	11800
	7	Silt clay	23.6	7.0	5100	0.087	40.3	<20.0	5030
Wausau	8	Sand	8.8	6.08	66800	0.014	24.7	<20.0	642
	9	Sand	11.3	7.12	38000	0.016	26.2	<20.0	614
* ***Mean Total Organic Carbon***									


Milwaukee


Madison


Wausau

For each soil sample (in all groups), a container with three identical specimens, either as-received steel, steel-mortar, or sandblasted steel, was prepared. Just one of the soils, i.e. soil 9, was used for with the sandblasted specimens. The specimens were vertically embedded in soils (for steel-mortar specimens, mortars on top to simulate the real condition) and the container was sealed with a lid to minimize moisture loss.

A three-electrode measurement setup, as shown in Figure 3.4, including a specimen as the working electrode, a saturated calomel electrode (SCE) as the reference electrode, and a 316-stainless steel sheet as the counter electrode, was used for the electrochemical test. To evaluate the probability of the corrosion of the specimens, the corrosion potential of all specimens was measured versus SCE.

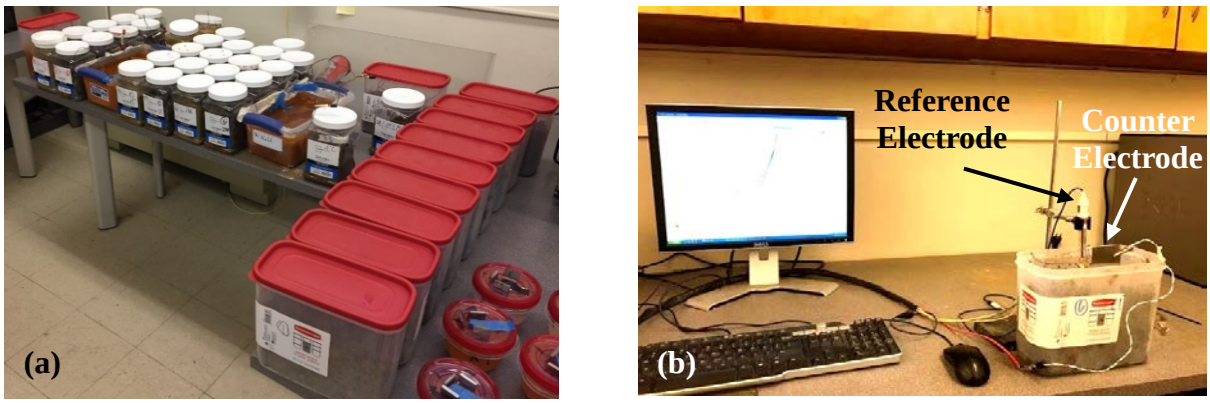

Figure 3.4 (a) All experiment cells; (b) One of the corrosion measurement cells

Linear Polarization Resistance (LPR) technique was used to determine the corrosion current densities of the steel specimens, by applied ±10mV potential over the corrosion potential and measure the resultant current. The LPR and potential measurements were started 24 hours after embedding the specimens in the soil. The cyclic polarization technique was used to evaluate the

susceptibility of the specimens to pitting corrosion. For all cyclic polarization tests, the potential scanned from -100 mV against open circuit potential to +500 mV versus the reference electrode and reversed to -100 mV versus the reference electrode with the scan rate of 0.166 mV/s [130].

It was hypothesized that when two identical steel specimens, one embedded in as-received soil and one in soil with the elevated chloride content, a galvanic corrosion was flown between them. To evaluate this hypothesis, steel specimens were embedded in two separate containers, one filled with as-received soil and the other filled with the same soil, with increased chloride content to 3% weight of the soil. Specimens were connected together by copper wires. 24 hours before conducting the experiment, the specimens were disconnected from each other; then the galvanic current between them was measured using Zero Resistance Ammetery (ZRA) technique.

The corrosion current density, i_{corr}, can be calculated from the measured R_p from the LPR tests, using the following equation:

$$R_p = B/I_{corr} \qquad \text{eq. 3.1}$$

$$i_{corr} = I_{corr}/A \qquad \text{eq. 3.2}$$

where B is the Stern-Geary constant and A is the corroded surface area. B can be calculated using eq. 3.3:

$$B = \beta_a \beta_{c\,/\,2.3} (\beta_a + \beta_c) \qquad (3.3)$$

where β_a and β_c are anodic and cathodic Tafel slopes. To measure these values, Tafel test was conducted on the specimens in each soil by polarizing the steel specimens ±500 mV versus their corrosion potential with a scan rate of 0.166 mv. s^{-1} [130]. The βa and βc were extracted from the results and used to calculate the Stern-Geary Constant, which was required to calculate the corrosion current densities from the polarization resistance (R_p) obtained by the LPR technique.

During repair and maintenance of the pile, it is probable to connect a new steel to the old corroded one. To study the change in corrosion of steel due to such condition, old and corroded steel was obtained from WisDOT and were connected to the new as-received specimens in a measurement cell with water. Epoxy coating on old rusted specimens provided the same exposure area as as-received specimens and prevented extraneous effects.

CHAPTER 4: RESULTS AND DISCUSSION

4.1. Corrosion Measurements

Table 4.1 shows the average Tafel slopes and the calculated Stern-Geary constants of the specimens in different soils. These values were used to calculate the corrosion current densities using R_p values obtained from the LPR measurements.

Table 4.1. Tafel slopes (βa and βc) and calculated Stern and Geary Constants (B)

Soil sample ID	βa	βc	B
1	0.53	0.21	0.03
2	0.31	0.44	0.04
3	0.57	0.51	0.13
4	0.33	050	0.06
5	0.49	0.36	0.06
6	0.38	0.43	0.05
7	0.43	0.34	0.05
8	0.23	0.40	0.02
9	0.38	0.31	0.03

Figures 4.1a and 4.1b show the corrosion potential values of the as-received and the steel-mortar specimens embedded in soils without addition of chloride, respectively.

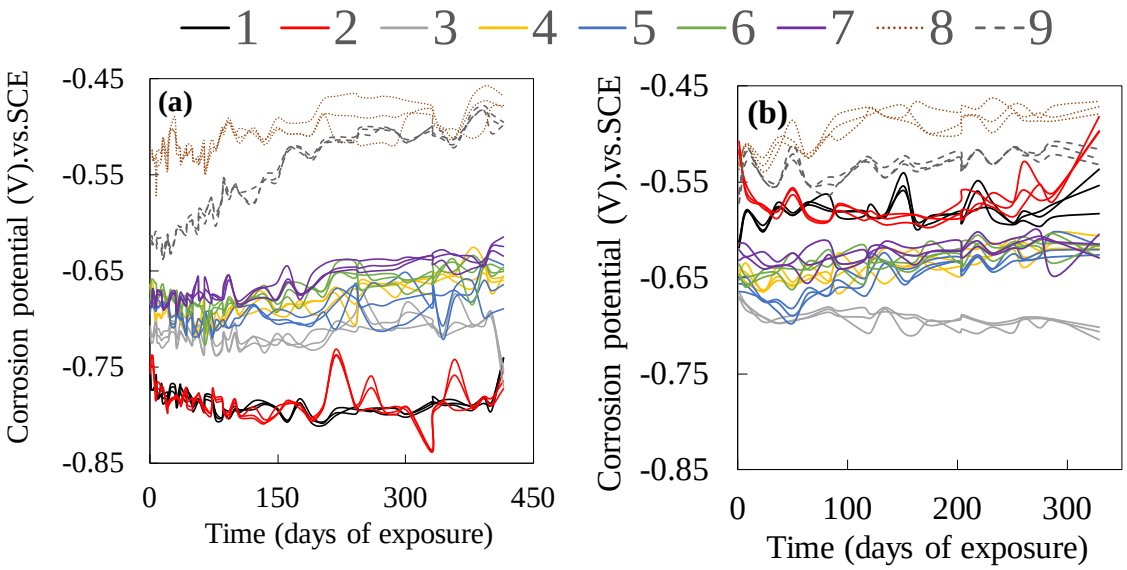

Figure 4.1. Corrosion potential values of (a) as-received and (b) steel-mortar specimens in 9 different soils (without addition of Cl).

Figures 4.2a and 4.2b show the corrosion potential values of the as-received and steel-mortar specimens embedded in soils with 3% chloride by weight of soil, respectively.

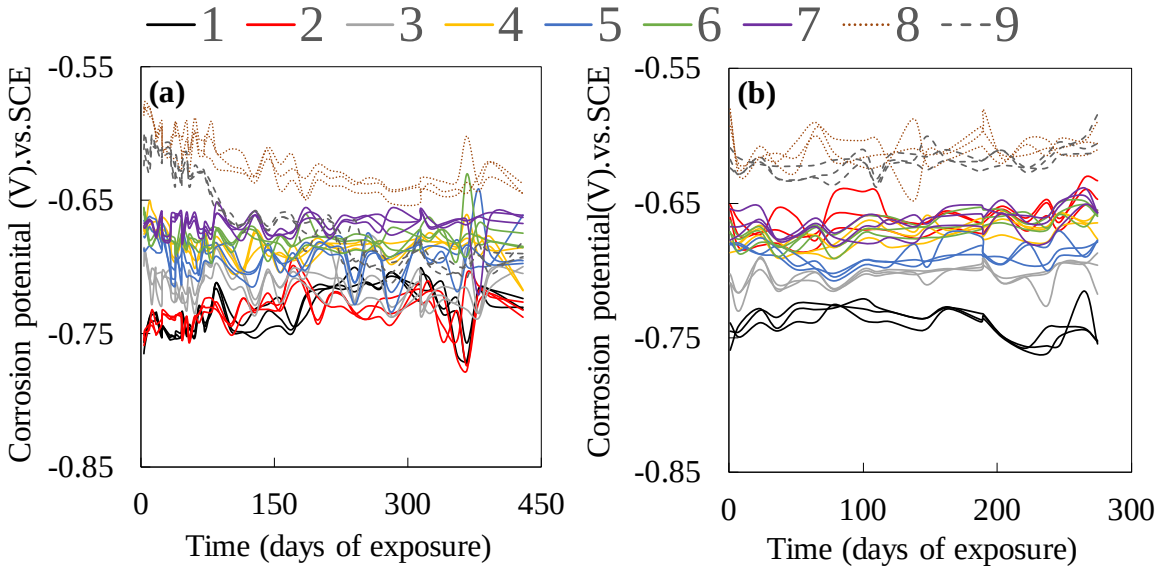

Figure 4.2. Corrosion potential values of (a) as-received and (b) steel-mortar specimens in 9 different soils (with 3% Cl by weight).

At the end of the experiments, the specimens (both as-received and steel-mortar) were removed from the soils. Then, pictures were taken from both sides of each specimen (Appendix A) and image analysis was carried out with the aid of ImageJ [131] and the corroded surface area on each specimen was measured. Table 4.2 shows the average corroded area for each specimen in different soils.

Table 4.2 Calculated corroded area of the specimens, after, they removed from the soils

Soil	**As-received**		Soil	**Steel-mortar**	
	Corrode area ($\times 10^{-3}$ m^{-2})			Corrode area ($\times 10^{-3}$ m^{-2})	
	As-received soil	Soil with 3% NaCl		As-received soil	Soil with 3% NaCl
1	0.85	1.48	1	0.34	1.44
2	0.68	1.97	2	0.32	0.91
3	2.15	2.78	3	2.06	2.48
4	1.63	2.32	4	1.02	1.84
5	1.84	2.44	5	1.41	2.34
6	1.53	2.21	6	0.65	1.79
7	1.20	2.04	7	0.43	1.68
8	0.16	1.33	8	0.13	0.40
9	0.17	1.41	9	0.26	1.08

The current destines were calculated, using the corroded areas given in Table 4.2 and the results are shown in Figures 4.3 and 4.4.

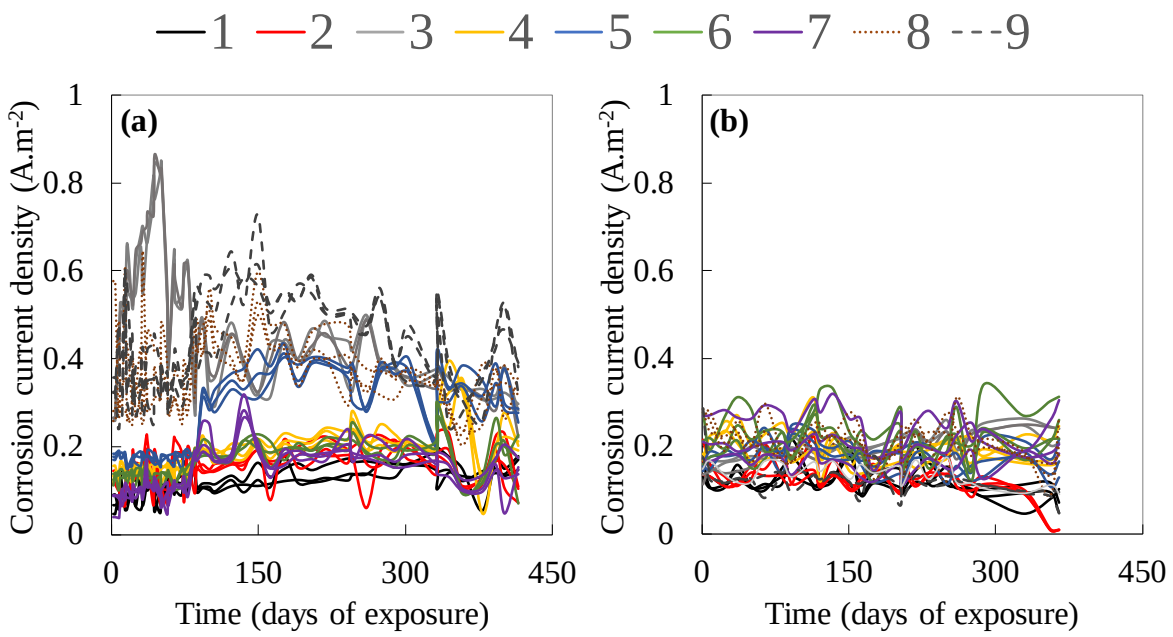

Figure 4.3 (a) Corrosion current densities of (a) as-received and (b) steel-mortar specimens in 9 different soils (without addition of Cl).

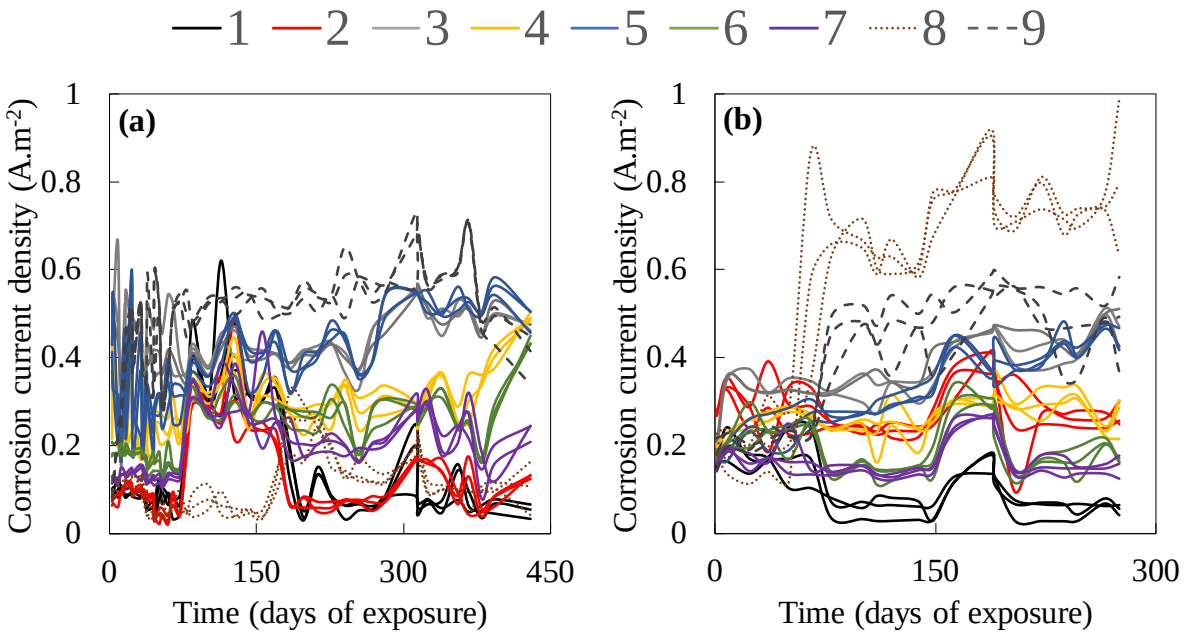

Figure 4.4 (a) Corrosion current densities of (a) as-received and (b) steel-mortar specimens in 9 different soils (with 3% Cl by weight).

At the end of the experiments, gravimetric analysis was conducted on all specimens and the weight loss was measured. In addition, the results of the corrosion current density measurements, Figures 4.3 and 4.4, were used to calculate the weight loss during the exposure time using Faraday's law, [132], the results of the measured and calculated weight loss are shown in Table 4.3 and Figure 4.5 shows the comparison between these values.

Table 4.3. Average calculated and measured weight loss of the specimens (AR: As-received specimen, SM: Steel-mortar specimen)

Soil	Calculated weight loss (g)				Measured weight loss (g)			
	As-received soil		Soil with 3% Cl		As-received soil		Soil with 3% Cl	
	AR	SM	AR	SM	AR	SM	AR	SM
1	2.15	0.34	4.30	3.97	2.60	0.92	5.53	4.42
2	2.14	0.34	2.78	1.73	2.98	0.94	3.70	2.43
3	7.40	3.29	13.12	6.45	6.76	2.18	10.38	7.00
4	3.39	1.60	7.68	6.38	3.75	1.37	9.60	8.72
5	5.86	2.07	11.21	5.29	4.82	2.00	10.27	6.82
6	2.81	1.16	8.17	7.40	2.47	2.58	9.73	8.97
7	1.98	0.71	6.71	5.92	2.45	0.73	7.19	6.28
8	2.60	1.23	10.62	14.65	3.01	1.95	10.29	15.26
9	3.99	9.28	7.77	16.60	4.99	10.75	10.34	18.73

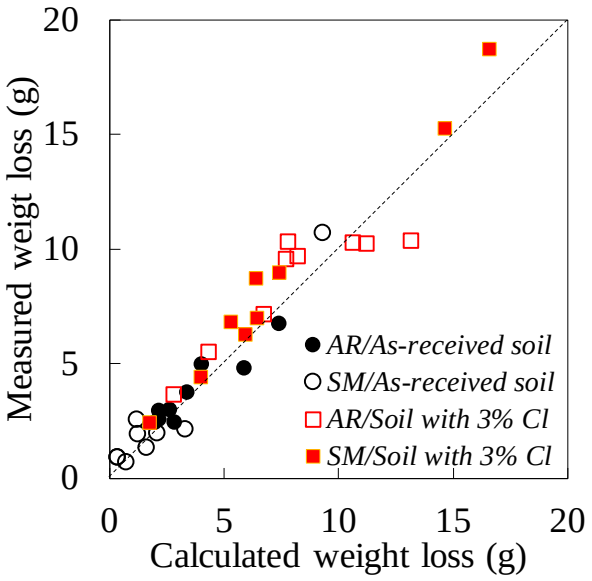

Figure 4.5. Comparison between the measured and calculated weight loss (AR: As-received specimen, SM: Steel-mortar specimen)

As can be seen, a good agreement exists between the measured and calculated values. The as-received steel specimens in as-received soil 3 showed the highest weight loss compare to the other as-received specimens. However, the steel-mortar specimens in soil 9 had the highest weight loss compared to the other steel-mortar specimens in both as-received soils and soils with 3% Cl. The high corrosion activity in soil 3 can be attributed to the level of sulfate in that soil (Table 3.2). However, this high corrosion activity was not observed for soil 5, which had highest sulfate content among all soil samples. It was hypothesized that the bacteria in the soil samples were responsible for such observation. Nonetheless, no data on the type and population of the bacteria were available to support this hypothesis. This requires further investigation.

To compare the two different types of specimens, the corrosion potentials and corrosion current densities of the steel-mortar specimens, in soils without increasing their chloride content, were plotted against the same values for the as-received steel specimens as shown in Figures 4.6.

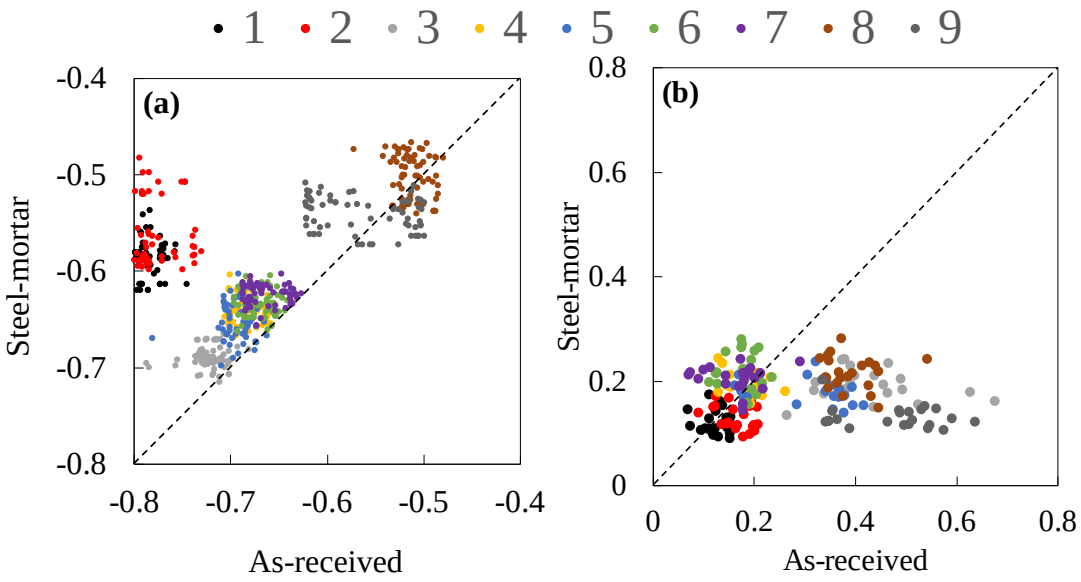

Figure 4.6. Comparison of (a) corrosion potential (V) values and (b) corrosion current densities ($A.m^{-2}$) between as-received specimens and steel-mortar specimens in 9 different soils (without addition of Cl).

As can be seen, the corrosion potential values for as-received and steel-mortar specimens were comparable, except for soils 1 and 2. However, in general, the corrosion current densities of the as-received specimens were higher than those for the steel-mortar specimens. It can be concluded that overall, steel-mortar specimens indicated less corrosion activity compared to the as-received steel specimens in the as-received soils.

Comparison of the corrosion current density and corrosion potential values of as-received steel and steel-mortar specimens in soils with elevated chloride content are shown in Figure 4.7.

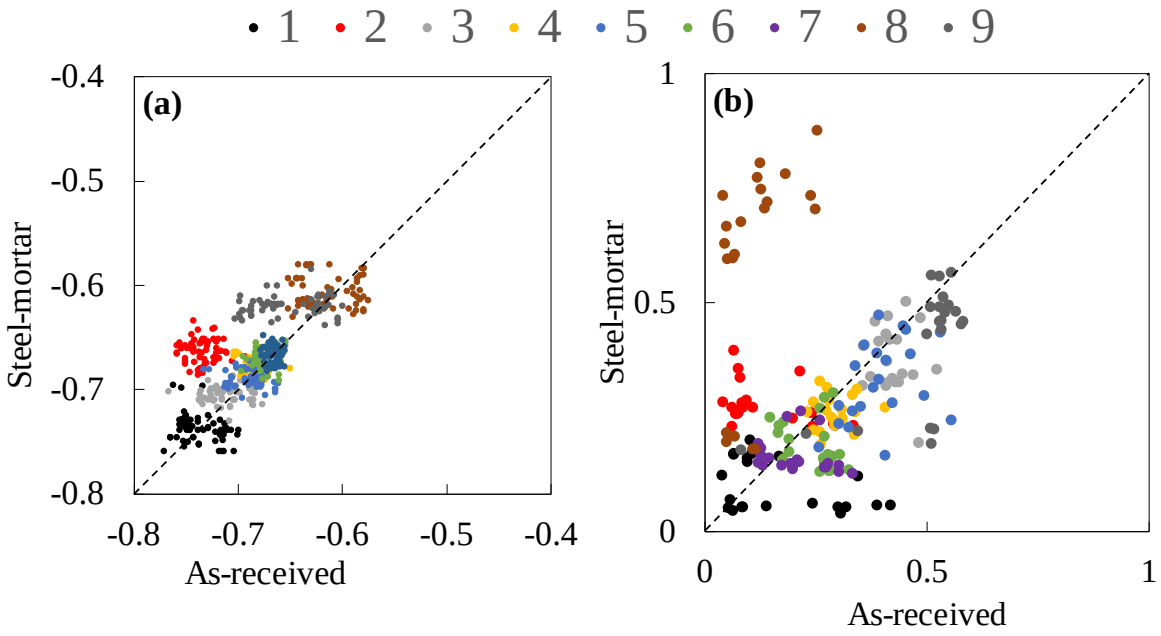

Figure 4.7. Comparison of (a) corrosion potential (V) values and (b) corrosion current densities ($A.m^{-2}$) between as-received specimens and steel-mortar specimens in 9 different soils (with 3% Cl by weight).

As can be seen, after addition of chloride, all specimens showed comparable corrosion potential values. The corrosion densities of the steel-mortar specimens were also comparable, except for soils 8 and 9, which were considerably higher for steel-mortar specimens.

Figures 4.8 and 4.9 show the results of the cyclic polarization experiments on one of the specimens after 2 days and 420 days exposure to as-received soils and soils with the elevated chloride content.

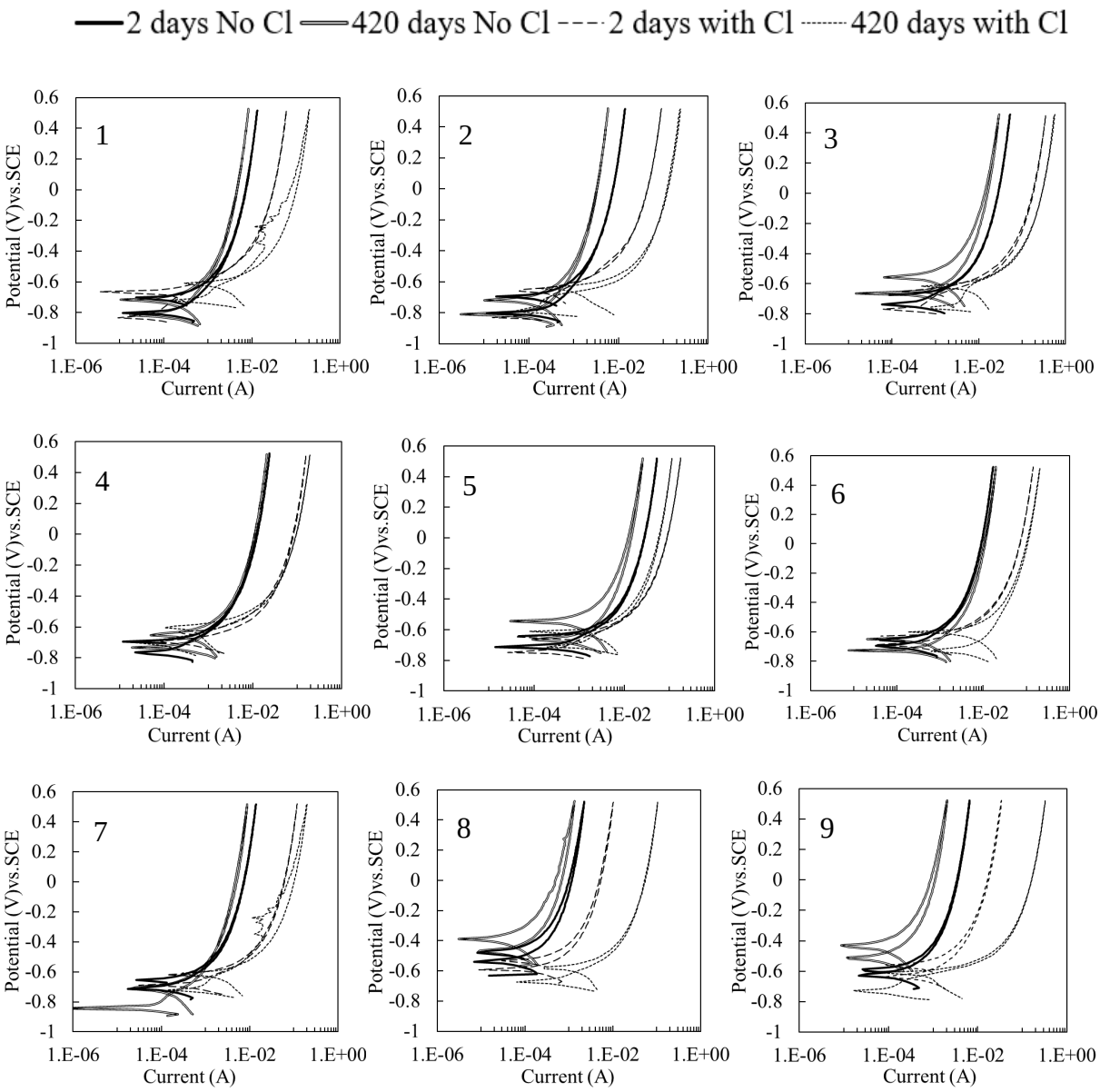

Figure 4.8. Cyclic polarization plots for one of the as-received specimens in each soil (1 to 9 according to Table 3.2), after 2 days and 420 days exposure to chloride free and 2 days and 420 days exposure to 3% by weight chloride contaminated soils.

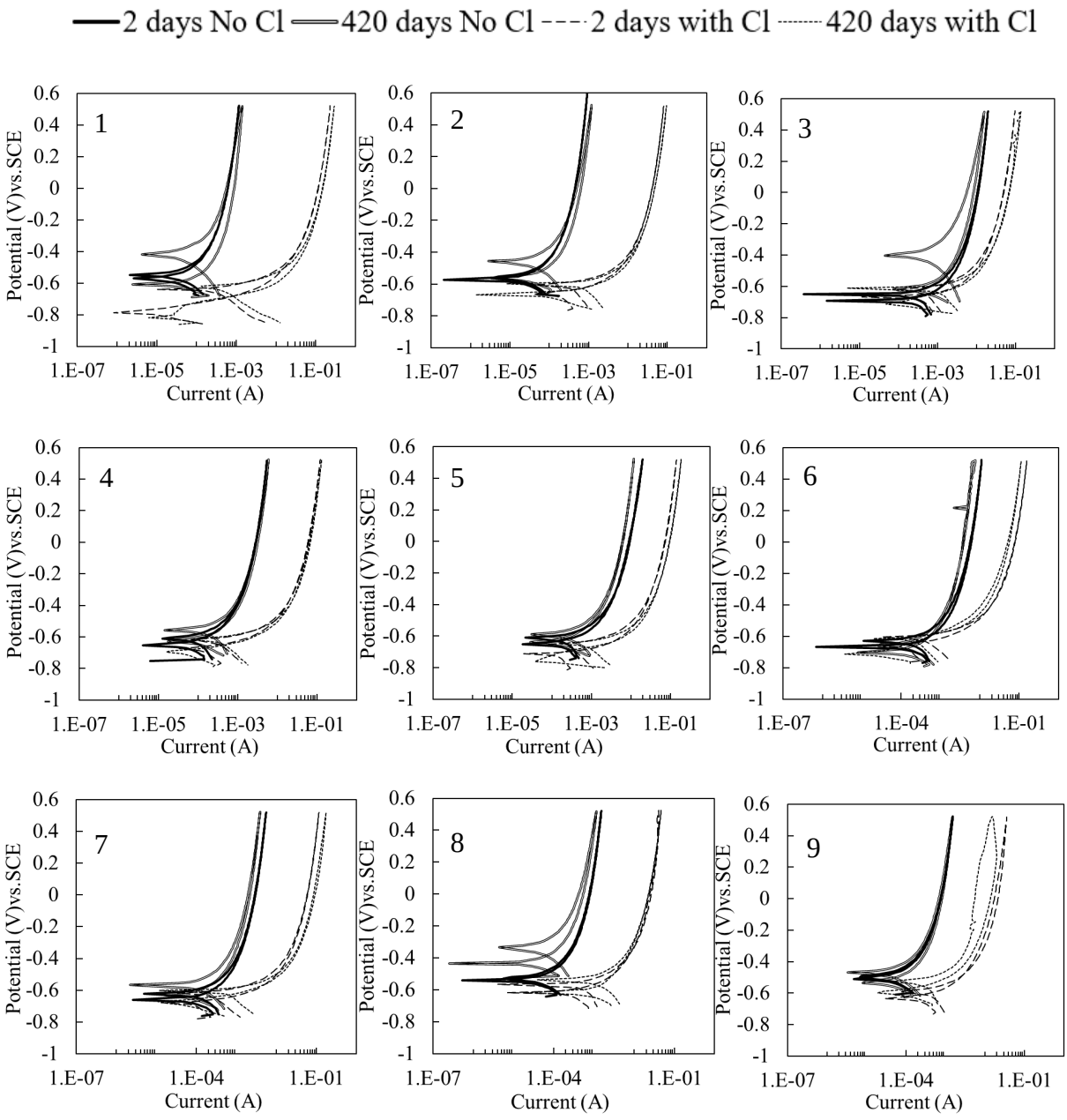

Figure 4.9. Cyclic polarization plots for one of the steel-mortar specimens in each soil (1 to 9 according to Table 3.2), after 2 days and 420 days exposure to chloride free and 2 days and 400 days exposure to 3% by weight chloride contaminated soils.

The addition of salt caused significant changes in all specimens. For steel specimens, as time of exposure increased, corrosion activity also increased.

The galvanic current between specimens in the soils with and without addition of chloride was calculated using the results from the ZRA test and are shown in Figure 4.10. As can be seen, galvanic current existed in all cases and the current flowed from specimens in soils with elevated chloride content to the specimens in the as-received soils. The galvanic current was minimum in soils 3 and 5. Galvanic behavior depends on different factors such as geometry, surface area ratio and mass transport [133]. However, since the parameters in this experiment were similar for both specimens in the coupled cell, the galvanic behavior could only be attributed to the difference in the chloride levels in the soil; with the chloride acting as an oxidizing species.

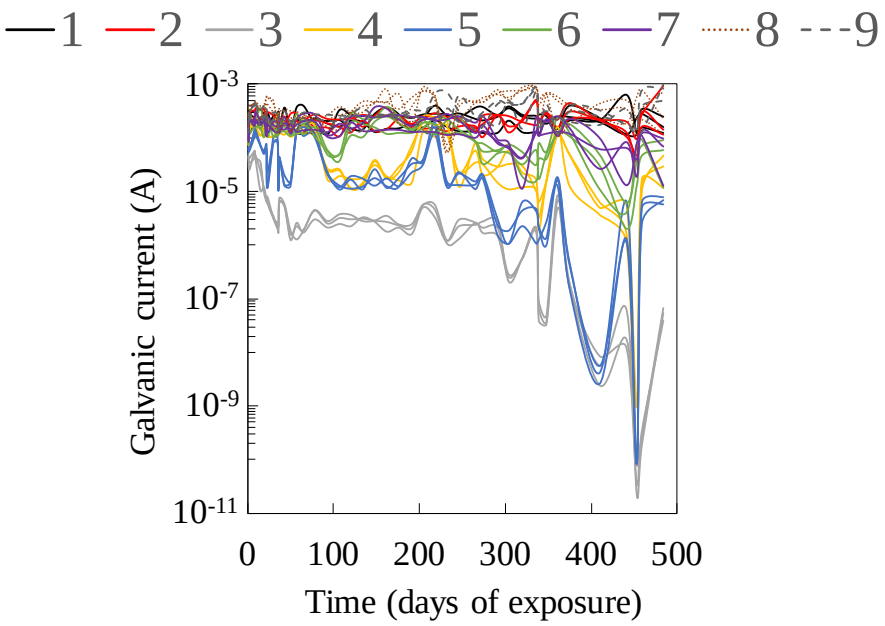

Figure 4.10. Galvanic current, obtained from the ZRA test on as-received specimens in chloride free and 3% by weight chloride contaminated soils.

Figure 4.11 shows the corrosion potential and the corrosion current density values of the as-received and sandblasted specimens embedded in soil 9. As can be seen, the sandblasted specimens showed more positive potential values compared to that for the as-received specimens. The sandblasted specimens also showed considerably lower corrosion activity compared to the as-

received specimens. These results corresponded well with the results from corrosion potential measurements.

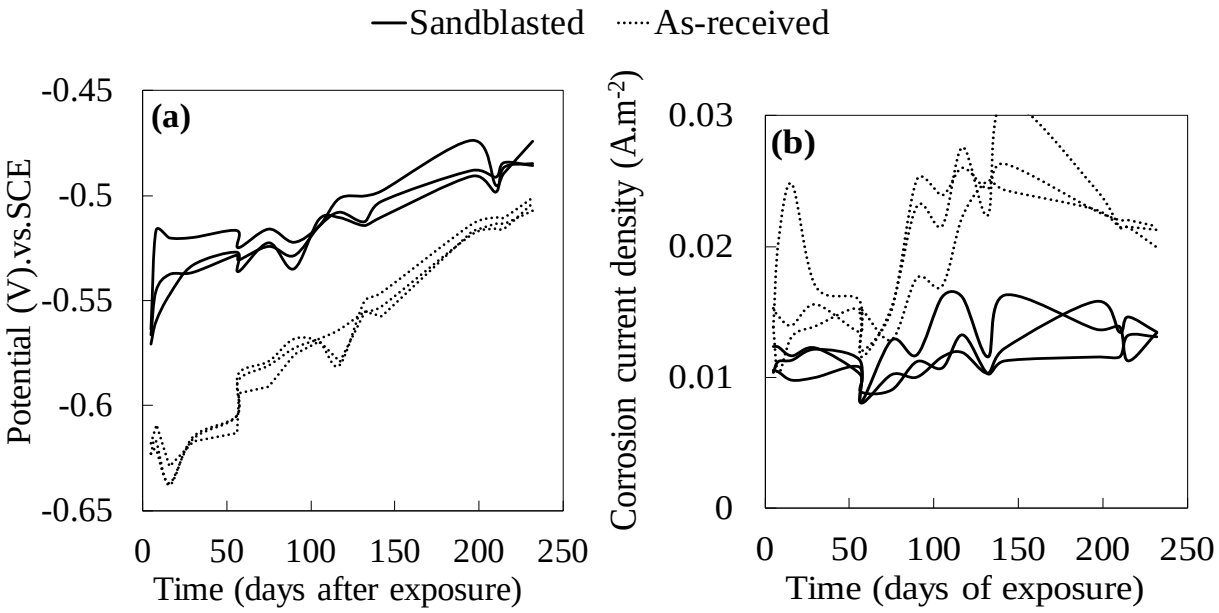

Figure 4.11. (a) Corrosion potential values and (b) corrosion current densities of the as-received and sandblasted specimens in soil 9.

The mass loss in each specimen can be calculated by determining the area under each curve in Figure 4.12 and using Faraday's law [13]. Figure 4.13 shows the calculated mass loss of the specimens. The mass loss of the as-received specimens was approximately 70.5% higher than that for the sandblasted specimens. It should be noted that this observation might be valid only for the exposure condition used in this investigation. These results clearly showed that when the surface of the steel was sandblasted, the corrosion rate decreased significantly.

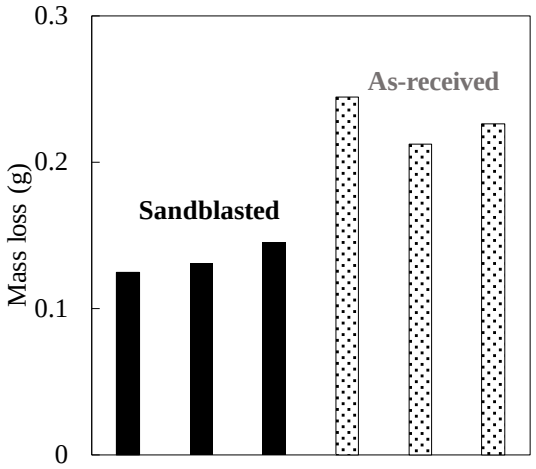

Figure 4.12. Calculated mass loss for sandblasted and as-received steel specimens during 232 days of being embedded in the soil.

Figure 4.13 shows the corrosion potential and corrosion current densities of both new (as-received) and old rusted steel in water; vertical dash line represents the date of chloride addition. As can be seen, after addition of chloride, new steel showed more negative corrosion potential, (more corrosion activity) compared to the old rusted specimens. The old rusted specimens showed higher corrosion current densities compared to the as-received specimens since the first day of the addition of chlorides.

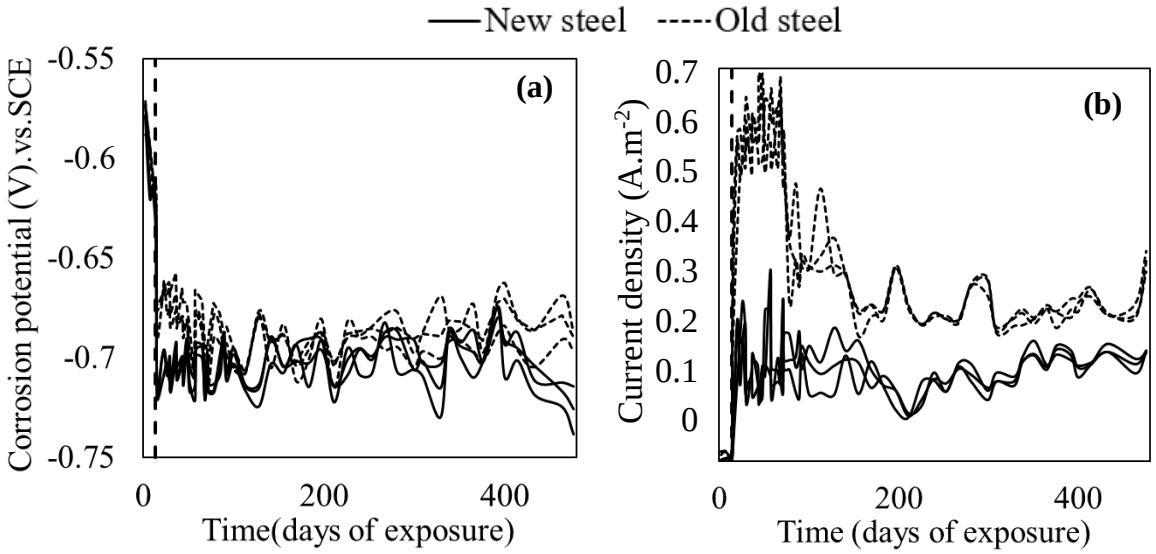

Figure 4.13. (a) Corrosion potential values and (b) corrosion current densities of new and old steels in water. Vertical dash line represents the data of chloride addition.

Figure 4.14 shows the galvanic corrosion current of coupled old and new steel in chloride free and 3% by weight chloride contaminated tap water. As can be seen, galvanic current existed in all cases and the current flowed from specimens in water both with and without chlorides. Coupled specimens exposed to the chloride-contaminated water showed higher galvanic current compared to those in the chloride-free water. The direction of the current was from old to new specimens, indicating enhancing the increase in corrosion on the old specimens.

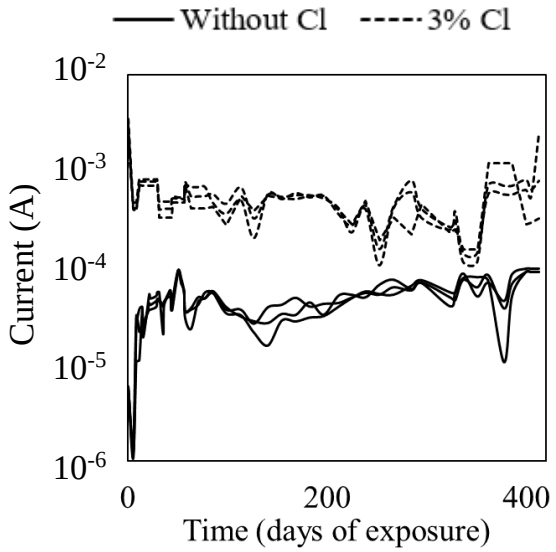

Figure 4.14. Galvanic current, obtained from the ZRA test on new and old steel in chloride-free and 3% chloride contaminated tap water.

4.2. GRNN Model

4.2.1. Construction of the GRNN

The MATLAB codes were written for the generalized regression algorithm. GRNNs consisted two steps. The first step was the training the neural network. The physicochemical variables of soil samples, as well as exposure time of specimens in soils, were used as input, corresponding to X in the equation 2.3, and the experimental data from measurements of corrosion current densities

and corrosion potentials of the steel specimens were used as training input, corresponding to Y_i in equation 2.3. The simulated corrosion current densities or corrosion potentials were the outputs of the network as shown in layer four in Figure 4.15. Since the input parameters were in different ranges, these parameters were normalized within 0.1-1 ranges to prevent the simulated Euclidean distance from being driven too far. The data from 5 months of measurements were used for building the model. The corrosion current densities and corrosion potential values measured from three identical specimens (Figures 4.6) were combined. 70% of these data were selected randomly and used for training, the same data were used for validation, and the rest 30% were used for testing. In this model, the network structure with spread constant σ=1 provided the best performance, i.e. minimum MSE.

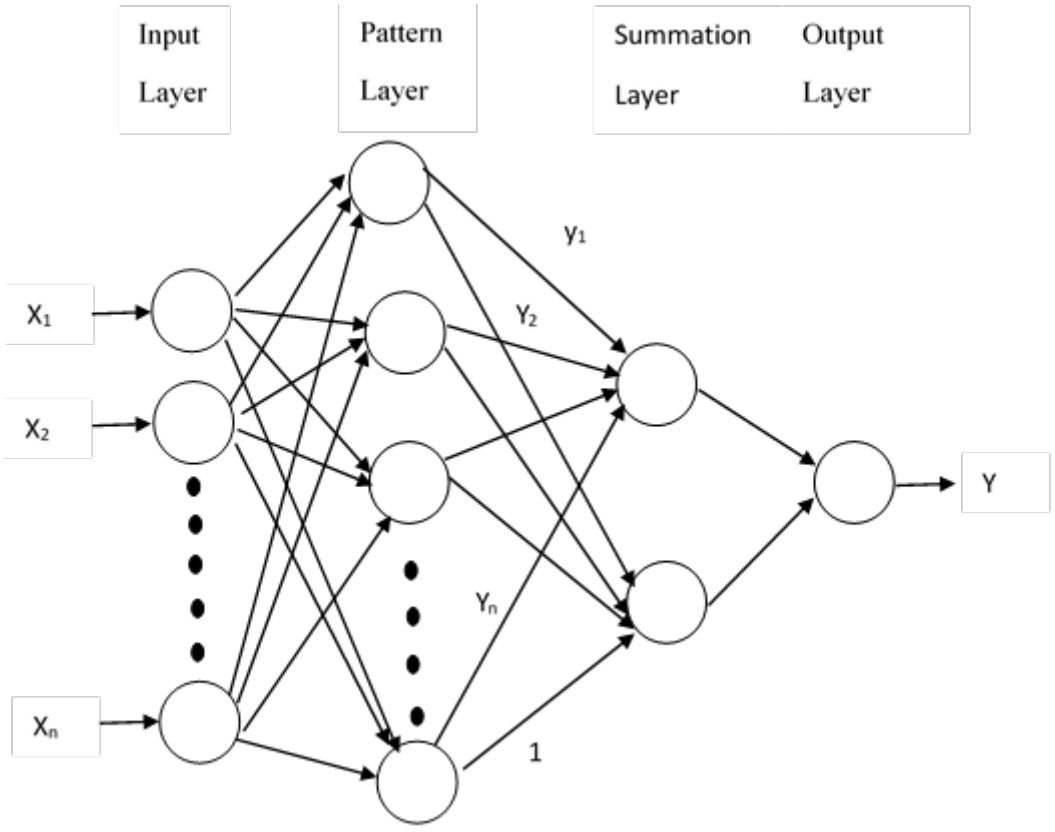

Figure 4.15. Schematic diagram of GRNN architecture.

4.2.2. Training and Testing of the Original Data

Table 4.4 shows the correlation coefficient (R^2), MSE and MAPE obtained from the GRNN model.

Table 4.4. R^2, MSE and MAPE calculated using the information obtained from the GRNN model.

Training set	Correlation coefficient (R^2)	MSE	MAPE (%)
	0.9995	0.0005159	0.4031
Corrosion current density training set	0.9983	0.001645	1.420
HCP validation set	0.9936	0.0008545	0.4471
Corrosion current density validation set	0.9633	0.03127	12.948
HCP Testing set	0.9990	0.006920	1.165
Corrosion current density testing set	0.9979	0.001879	1.565

As can be seen, statistically, the GRNN model could account for more than 96% of the variance of the corrosion current densities and corrosion potential values of the steel specimens embedded in different soils. It can also be noted that the MSE and MAPE indexes of corrosion potential values estimated by GRNN models were both less than those of corrosion current densities for training, validation, and testing; indicating that the prediction accuracy of corrosion potential values was greater than those of corrosion current densities. The results of R^2 corresponds well with MSE and MAPE, which reveals that the regression effect fitted by corrosion potential values was better than that of corrosion current densities.

4.2.3. Sensitivity Analysis

Sensitivity analysis explores the sensitivity of a model's outputs to changes in parameter values [134]. Sensitivity analysis is imperative for understanding the relationship between input parameters and outputs, testing the robustness of the output, and identifying errors in the model. Comparing the weights between nodes of input layer and nodes of hidden layer, showed that the magnitude of the weight of moisture and chloride contents were larger than the other parameters.

Thus, the sensitivity analysis conducted on the trained neural network to study the effects of moisture and chloride contents on the corrosion current densities and corrosion potential values. As can be seen in Figures 4.16 and 4.17, a positive linear relationship between both chloride and moisture contents and corrosion current densities; and a negative linear relationship between both chloride and moisture contents and corrosion potential values, indicated significant impact of these variables on the corrosion current densities and corrosion potential values of steel specimens in different soils.

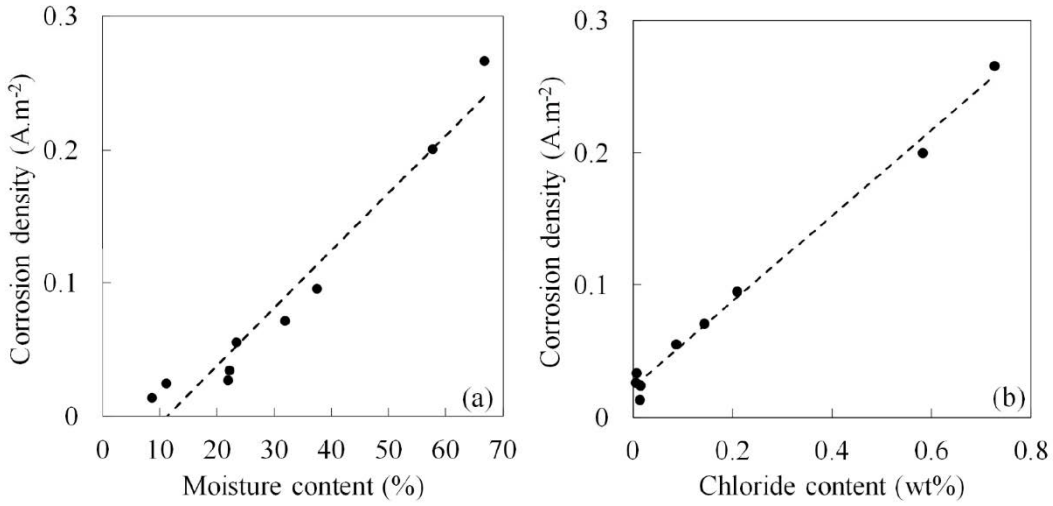

Figure 4.16. Effect of (a) moisture content and (b) chloride content of soil on the corrosion current densities.

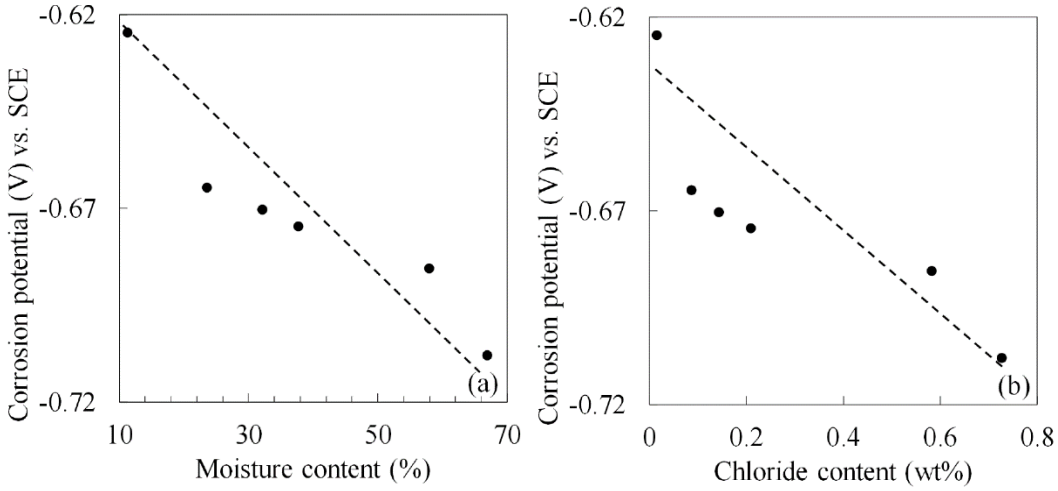

Figure 4.17. Effect of (a) moisture content and (b) chloride content of soil on corrosion potential values.

4.2.4. Case study I: Prediction of Corrosion Current Densities and Corrosion Potential Values of the Steel Specimens by Changing Chloride Concentration of the Soil

Based on the results of the sensitivity analysis, shown in Figures 4.16 and 4.17, increasing the chloride content of soil, significantly increases the corrosion activity of the embedded steel specimens. To experimentally explore the impact of increasing the chloride content on the corrosion activity of the steel specimens and to evaluate the performance of GRNN model on the prediction of corrosion behavior, the chloride content of the soils was increased to 3% by weight and laboratory experiments were conducted on the steel specimens.

Figures 4.18a and 4.18b show the comparison between the predicted and the experimentally measured corrosion current densities and corrosion potential values, respectively. The predicted results were achieved by changing one of the input vectors (chloride content) in the algorithm in the original GRNN model that described before.

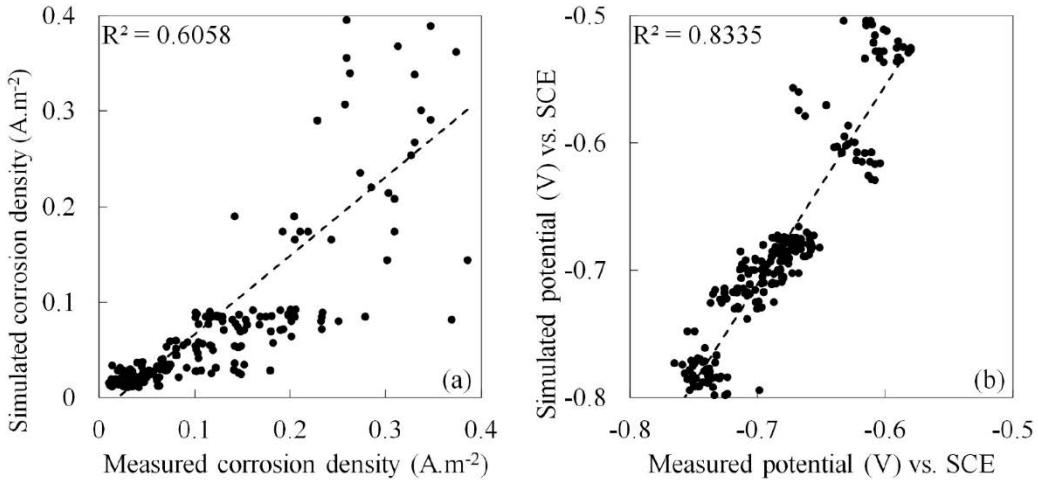

Figure 4.18. Comparisons of measured and predicted (a) corrosion current densities and (b) corrosion potential values after increasing the chloride concentration of soils to 3% by weight. Original GRNN model was used

The R^2 values of 0.605 and 0.833 for current densities and corrosion potential values, shown in Figure 4.18, indicated reasonable prediction by the model. However, to enhance the performance of the model, the model has undergone another training process.

The maximum value of the chloride concentration of the as-received soils was 0.727%, which was 2.273% points less than that after increasing chlorides level to 3% by weight. This changing had a significant effect on the Euclidean distance and activation function in the original model. Thus, to improve the model, 50% of the soil parameter data after adding chloride as inputs as well as 50% of the corrosion current densities and corrosion potentials as outputs were combined with original data used for training, and the rest 50% was used for testing. Table 4.5 shows the GRNN performance for the steel specimens after this procedure.

Table 4.5. GRNN performance for the steel specimens after adding chloride.

Training set	Correlation coefficient (R^2)	MSE	MAPE (%)
HCP training set	0.9997	0.0004368	0.04031
Corrosion current density training set	0.9905	0.03954	12.57
HCP validation set	0.9986	0.001526	1.469
Corrosion current density validation set	0.9934	0.009839	5.623
HCP Testing set	0.9661	0.06375	27.59
Corrosion current density Testing set	0.8816	0.5691	47.63

Clearly, training the model significantly improved its prediction capability. The model was run using the remaining data that were not used in the training and validation steps. The comparison between predicted, obtained from the newly trained model, and the measured data of steel specimens after increasing chloride concentration are shown in Figures 4.19a and 4.19b. As can be seen, after training the model, the results of the prediction were close to the directly measured values from the experiments and good correlation existed among the measured and the predicted values as shown in Table 4.5.

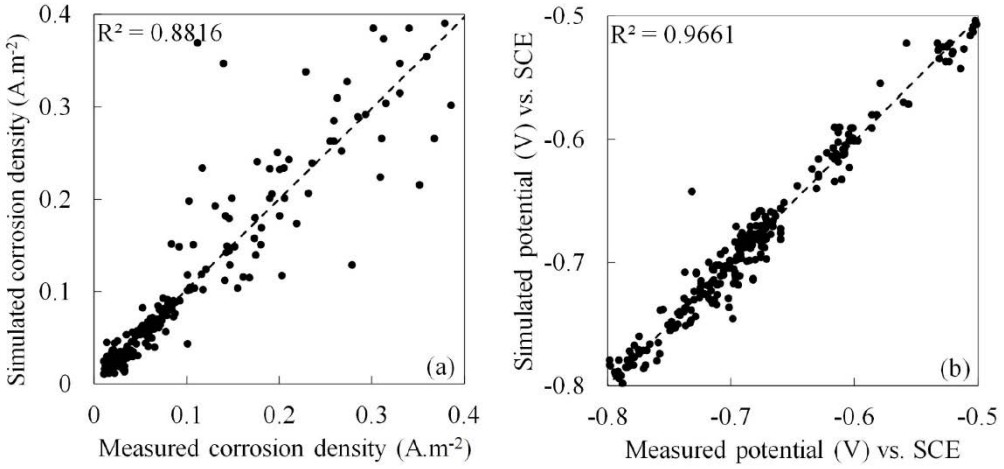

Figure 4.19. Comparisons of measured and predicted (a) corrosion current densities, and (b) corrosion potential values, after increasing the chloride concentration of soils to 3% by weight. The original GRNN model was trained again.

4.2.5. Case Study II: Prediction of the Corrosion Current Densities and Corrosion Potential Values of the Steel specimens in Different Soils ahead of the Experimental Measurements

To evaluate and validate the performance of the model in the realistic prediction of the corrosion behavior of the embedded steel specimens, the re-trained GRNN model described in Case Study I was used to predict the corrosion current densities and corrosion potential values of steel specimens in all soils 10 weeks ahead of the actual experimental measurements. Then, after the time was reached, the measurements were conducted, and the results were compared with the predicted values. As shown in Figures 4.20, the predicted values were very close to the measured values and the model can effectively predict the performance of steel specimens.

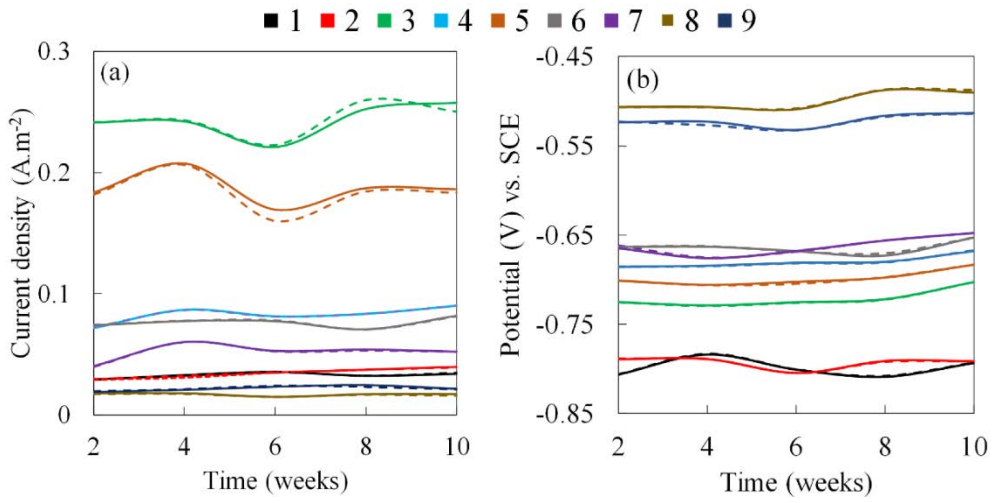

Figure 4.20. Comparisons of the measured and predicted (a) corrosion current densities and (b) corrosion potentials 10 weeks ahead of actual experimental measurements. Dash lines and solid lines represent the measured and the predicted data, respectively.

CHAPTER 5: CONCLUSIONS

- In general, (except soil 8-(Milwaukee-Silt clay)) the steel-mortar specimens and as-received specimens showed comparable corrosion activities in both as-received soils and soils with elevated chloride content.
- As-received steel specimens in as-received soil 3 (Milwaukee-Clay) showed highest corrosion current densities compared to other as-received specimens.
- When chlorides were added, the steel-mortar specimens in soils 8 and 9 (Wausau-Sand) showed higher corrosion current densities compared to the other specimens.
- Corrosion potential values of all specimens remained relatively stable, both before and after addition of chlorides, while the corrosion current densities were increased after addition of the chlorides. Thus, based on this result, measuring just the corrosion potential was not an efficient and accurate method to evaluate the corrosion behavior of the steel in soil.
- The physiochemical parameters available for the soils could not be used to explain the observed behaviors. It was hypothesized that the synergistic activity of the chlorides and SRB was the reason of significant increase in the corrosion rates of steel in soil 9 (Wausau-Sand). However, no information was available on the type and population of the bacteria in the soils to support this hypothesis.
- The galvanic corrosion was also observed between steel in soils with the same chemistry but different chloride contents.
- Sandblasting significantly enhanced the corrosion resistance of the steel in soil compared to as-received specimens.

- Old steel specimens retrieved from the bridge showed higher corrosion activity compared to the new as-received steel. This point needs to be considered during repair and maintenance if such combination is expected.
- A very good correlation between the corrosion potential values and corrosion current densities obtained from the GRNN model and the experimental measurements was observed for the as-received soils.
- The sensitivity analysis was conducted on two input parameters, i.e. chloride content and moisture content. Results showed that changing these parameters had a significant impact on the corrosion current densities and corrosion potential values of the steel specimens. The chloride content of the as-received soils increased and the original model was run.
- Results showed that while the initial model could predict the corrosion activity of the steel specimens, the accuracy of the prediction was not very high. The model was trained again and the performance of the new model in predicting the corrosion activity of the steel in the soils with elevated chloride content was enhanced significantly.
- The model was used to predict the corrosion current densities and corrosion potential values of the steel specimens ahead of the actual experimental measurements and the results showed that the model is highly capable of predicting these values.

APPENDIX A

PICTURES OF THE CORRODED SPECIMENS

As-received soil (with no Cl addition)/as-received steel

Soil 1

Specimen 1

Side A

Side B

Specimen 2

Side A

Side B

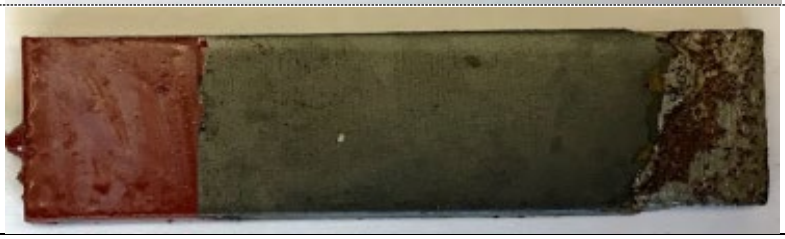

Specimen 3

Side A

Side B

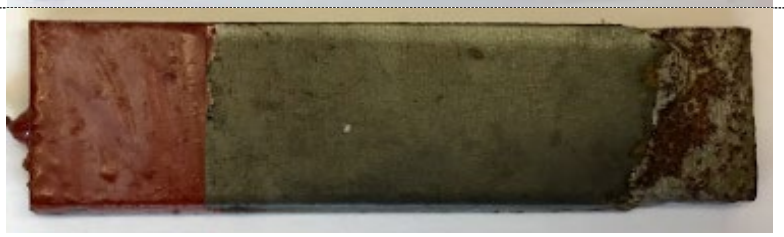

Soil 2

Specimen 1

Side A

Side B

Specimen 2

Side A

Side B

Specimen 3

Side A

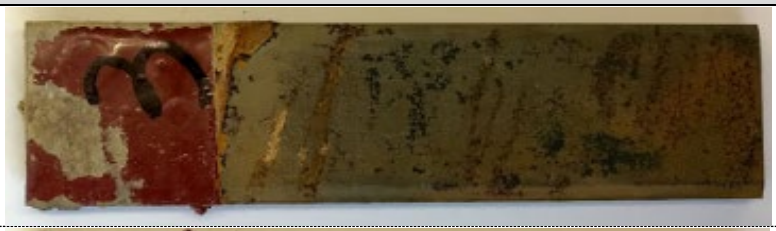

Side B

Soil 3

Specimen 1

Side A

Side B

Specimen 2

Side A

Side B

Specimen 3

Side A

Side B

Soil 4

Specimen 1

Side A

Side B

Specimen 2

Side A

Side B

Specimen 3

Side A

Side B

Soil 5

Specimen 1

Side A

Side B

Specimen 2

Side A

Side B

Specimen 3

Side A

Side B

Soil 6

Specimen 1

Side A

Side B

Specimen 2

Side A

Side B

Specimen 3

Side A

Side B

Soil 7

Specimen 1

Side A

Side B

Specimen 2

Side A

Side B

Specimen 3

Side A

Side B

Soil 8

Specimen 1

Side A

Side B

Specimen 2

Side A

Side B

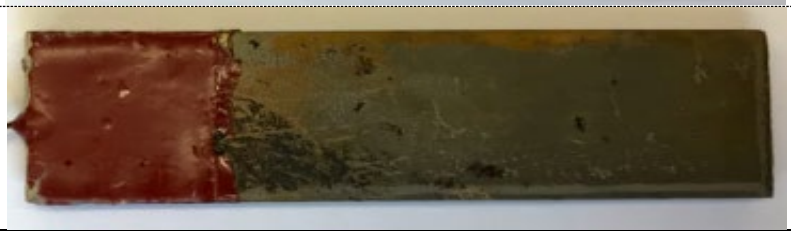

Specimen 3

Side A

Side B

Soil 9

Specimen 1

Side A

Side B

Specimen 2

Side A

Side B

Specimen 3

Side A

Side B

As-received soil (with no Cl addition)/ steel-mortar

Soil 1

Specimen 1

Side A

Side B

Specimen 2

Side A

Side B

Specimen 3

Side A

Side B

Soil 2

Specimen 1

Side A

Side B

Specimen 2

Side A

Side B

Specimen 3

Side A

Side B

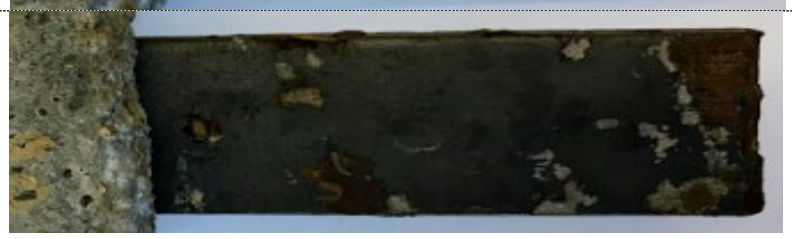

Soil 3

Specimen 1

Side A

Side B

Specimen 2

Side A

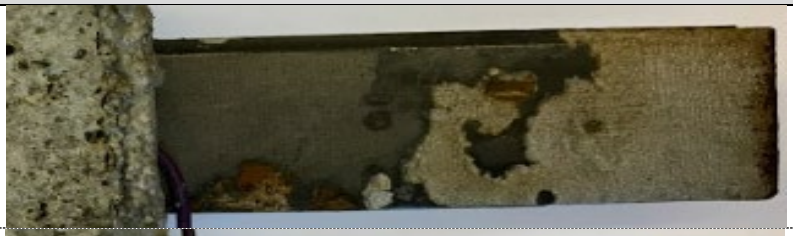

Side B

Specimen 3

Side A

Side B

Soil 4

Specimen 1

Side A

Side B

Specimen 2

Side A

Side B

Specimen 3

Side A

Side B

Soil 5

Specimen 1

Side A

Side B

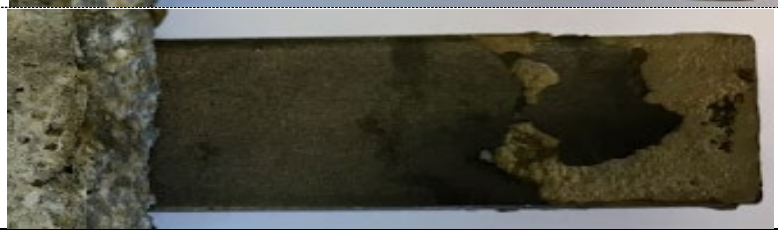

Specimen 2

Side A

Side B

Specimen 3

Side A

Side B

Soil 6

Specimen 1

Side A

Side B

Specimen 2

Side A

Side B

Specimen 3

Side A

Side B

Soil 7

Specimen 1

Side A

Side B

Specimen 2

Side A

Side B

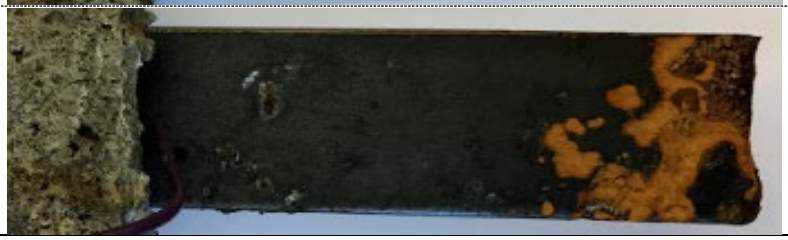

Specimen 3

Side A

Side B

Soil 8

Specimen 1

Side A

Side B

Specimen 2

Side A

Side B

Specimen 3

Side A

Side B

Soil 9

Specimen 1	
Side A	
Side B	

Specimen 2	
Side A	
Side B	

Specimen 3	
Side A	
Side B	

<u>Soil with Cl addition/as-received steel</u>

Soil 1

Specimen 1

Side A

Side B

Specimen 2

Side A

Side B

Specimen 3

Side A

Side B

Soil 2

Specimen 1

Side A

Side B

Specimen 2

Side A

Side B

Specimen 3

Side A

Side B

Soil 3

Specimen 1

Side A

Side B

Specimen 2

Side A

Side B

Specimen 3

Side A

Side B

Soil 4

Specimen 1

Side A

Side B

Specimen 2

Side A

Side B

Specimen 3

Side A

Side B

Soil 5

Specimen 1

Side A

Side B

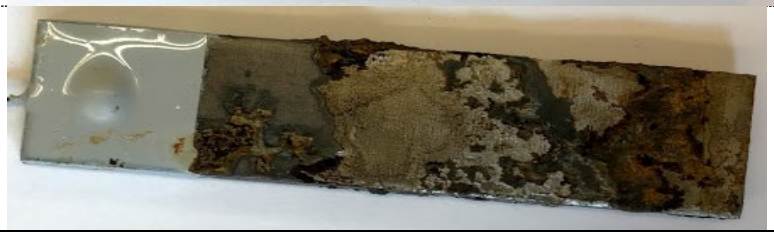

Specimen 2

Side A

Side B

Specimen 3

Side A

Side B

Soil 6

Specimen 1

Side A

Side B

Specimen 2

Side A

Side B

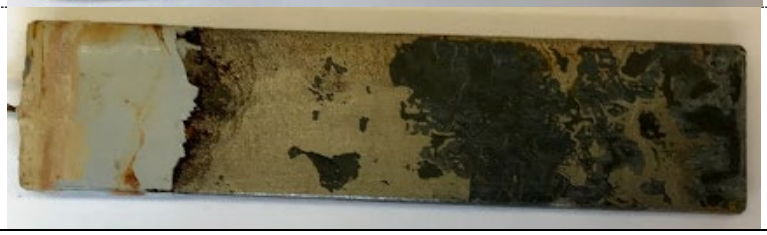

Specimen 3

Side A

Side B

Soil 7

Specimen 1

Side A

Side B

Specimen 2

Side A

Side B

Specimen 3

Side A

Side B

Soil 8

Specimen 1

Side A

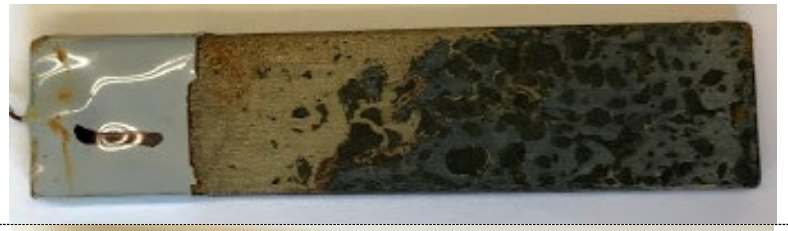

Side B

Specimen 2

Side A

Side B

Specimen 3

Side A

Side B

Soil 9

Specimen 1

Side A	
Side B	

Specimen 2

Side A	
Side B	

Specimen 3

Side A	
Side B	

<u>Soil with Cl addition/ steel-mortar</u>

Soil 1

Specimen 1

Side A

Side B

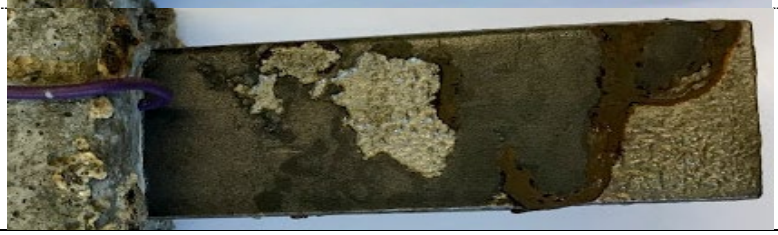

Specimen 2

Side A

Side B

Specimen 3

Side A

Side B

Soil 2

Specimen 1

Side A

Side B

Specimen 2

Side A

Side B

Specimen 3

Side A

Side B

Soil 3

Specimen 1

Side A	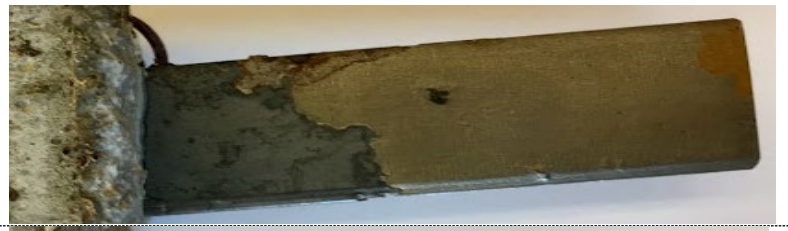
Side B	

Specimen 2

Side A	
Side B	

Specimen 3

Side A	
Side B	

Soil 4

Specimen 1

Side A

Side B

Specimen 2

Side A

Side B

Specimen 3

Side A

Side B

Soil 5

Specimen 1

Side A

Side B

Specimen 2

Side A

Side B

Specimen 3

Side A

Side B

Soil 6

Specimen 1

Side A

Side B

Specimen 2

Side A

Side B

Specimen 3

Side A

Side B

Soil 7

Specimen 1

Side A

Side B

Specimen 2

Side A

Side B

Specimen 3

Side A

Side B

Soil 8

Specimen 1

Side A

Side B

Specimen 2

Side A

Side B

Specimen 3

Side A

Side B

Soil 9

Specimen 1

Side A

Side B

Specimen 2

Side A

Side B

Specimen 3

Side A

Side B

APPENDIX B

FINDINGS FROM PREVIOUS REPORTS

B1. Corrosion Study of Piles in Salt Lake Valley, Utah

A study to evaluate corrosion rates was conducted using pile foundations abandoned during the reconstruction of I-15 through Salt Lake Valley, Utah. Corrosion rates were measured for 20 piles extracted from five sites after service lives of 34–38 years. Measurements were made of soil index properties, resistivity, pH, cation/anion concentrations, and water table elevation. The critical zone for corrosion was typically located within the groundwater fluctuation zone; but correlations with soil properties were generally poor. Despite low resistivity, average corrosion rates for pile caps in native soil were typically between 2 and 9 μm/year with a maximum of 19 μm/year and did not pose any structural integrity problems. Nevertheless, for abutment piles where chloride concentration was very high, the average pile corrosion rate increased to 13 μm/year. The corrosion rates were relatively constant with depth. Despite the low resistivity and the high chloride and sulfate concentrations, the maximum measured corrosion rate for Piles 1–3 was only 6 μm/year on Pile 3 at a depth of 2.59 m (8.50 ft) below the pile cap. Within the fill, the average corrosion rate for Piles 19 and 20 was only about 13 μm/year with a standard deviation of 2.1, despite the fact that the resistivity was less than 500 Ω cm, the chloride concentration averaged approximately 2,100 ppm, and the soil consisted of moist silty clay. The high chloride content is likely a result of deicing salt used heavily on the pavement during winter months.

The maximum measured corrosion rate for abutment piles driven through fill and into native soil at the 118th South site was considerably higher with an average corrosion rate of 13 μm/ year in the fill, 22 μm/ year in the native soil, and a maximum of 48 μm/ year in the native soil near the water table fluctuation zone. The high corrosion rates at this site can be attributed to high chloride content (due to deicing salt), low resistivity, and the piles being driven through fill. The corrosion

rate in the water table fluctuation zone was more sensitive to soil parameters than is the corrosion rate above and below this zone.

The corrosion rates dropped off below the maximum value; however, they did not decrease significantly with depth below the water table as would be expected. One possible reason for this discrepancy might be that the water table fluctuation zone was larger than estimated. However, further investigation provided strong evidence that biocorrosion was the cause of the higher corrosion rates at depth below the water table. Biocorrosion is typically caused by sulfate reducing bacteria (SRBs) which are commonly associated with saturated clays, a pH value near neutral and anaerobic conditions. SRBs also thrive where contaminants provide nutrients for bacterial growth and contribute to anaerobic conditions [135].

Table B1 shows the chemical testing of soil samples obtained at 1.5 ft to 2.5 ft intervals to a depth of 26.5 ft below the abutment footing. The chemical tests showed that changes in various chemical properties of the soil were evident with depth and especially at the native soil interface. Additionally, several parameters indicated the possibility of severe corrosion potential in the fill material.

Table B1. Chemical testing of soil samples obtained at 1.5 ft to 2.5 ft intervals to a depth of 26.5 ft below the abutment footing.

Depth Below Footing (ft)	pH	SO_4, ppm	Cl, ppm	Na, ppm	Ca, ppm	Mg, ppm	K, ppm	SAR	NO_3, ppm	NH_4, ppm	HCO_3, ppm	TDS, mg/l
0	7.89	31.86	3042.09	1750.50	237.00	224.70	121.80	19.47	1.92	2.28	110.18	7168
1.5	8.28	7.98	1922.42	1772.00	30.48	5.79	19.56	76.91	1.71	2.28	97.10	5888
3.5	7.75	50.13	2250.32	2864.00	323.60	67.27	65.84	37.73	4.16	3.79	147.19	9728
5	8.51	19.49	2505.25	2459.00	31.64	8.92	31.18	99.15	5.42	7.59	258.23	7552
7	8.28	19.93	2363.29	1841.50	46.31	14.43	33.81	60.37	3.20	13.66	147.19	6528
8.5	8.99	105.57	82.98	2568.00	25.10	18.05	59.73	95.06	4.98	9.86	390.45	8192
10.5	8.25	70.14	1518.54	1670.00	266.60	169.60	87.80	19.59	1.98	10.62	89.52	6848
12.5	7.53	74.79	1782.47	1512.50	490.60	232.70	105.00	14.03	1.68	11.38	72.31	6656
14.5	7.51	230.85	1477.56	1167.00	610.50	330.50	80.60	9.42	3.08	3.79	61.98	6624
17.5	7.50	290.79	2523.24	1500.00	568.30	488.80	145.20	11.09	10.54	28.83	1022.60	8704
18.5	7.99	52.98	1593.52	880.70	184.20	212.30	67.23	10.44	1.32	48.56	221.68	4800
20.5	7.87	46.96	1531.54	1488.16	350.30	358.80	60.35	13.29	1.68	15.18	64.04	6144
22.5	7.85	38.94	1420.57	798.20	215.70	214.80	71.63	9.16	1.83	12.14	84.11	4416
24.5	7.91	14.48	532.84	464.10	67.92	68.10	43.27	9.47	2.98	9.86	104.03	1920
26.5	8.11	18.86	418.87	328.50	65.73	60.79	39.67	6.99	3.71	13.61	111.56	1696

In summary, sites that have measured soil parameters where the pH is less than or equal to 5 or greater than 8.5, the resistivity lower than 340 Ω.cm, or a chloride concentration greater than 450 ppm may experience very aggressive pile corrosion and steps may need to be taken to prevent excessive corrosion.

B2. Phase 4 Subsurface Corrosion Investigation for CTH AB over I - 39/I - 90 (B - 13 - 139), McFarland, Wisconsin

The fill material located within the north abutment consisted of a reddish brown/tan, fine grained sand with occasional gravel and cobbles. Near the south abutment, the fill material was made up of sand similar to that on the north side, but also with slightly plastic silty clay which was a darker brown. All of the fill material observed was moist but not saturated. No industrial fill was observed during this investigation. The only potential evidence of contamination found was a slight chemical odor detected in the southern abutment soil samples. The fill conditions observed at the north and south abutments were consistent throughout the extent of their respective excavations. Of the 24 piles, a large majority had areas of pitting, surface corrosion and several had areas of

complete loss on the edges of the H-pile flanges. Table B2 shows the chemical analytical results of soils in this project.

Table B2. Soil Analytical Results CTH AB over I39/I90 - North and South Abutments (B-13-139) McFarland, Dane County, Wisconsin WISDOT ID #1007-10-81

SAMPLE ID	SAMPLE DEPTH (ft. bgs)	DATE AND TIME COLLECTED	SOIL COMPOSITION	COLOR	MOISTURE/ODOR	CORROSION CHEMISTRY					
						PERCENT MOISTURE (%)	pH (std. units)	RESISTIVITY (ohms-cm)	CHLORIDE (mg/kg)	SULFATE (mg/kg)	MEAN TOTAL ORGANIC CARBON (mg/kg)
P-4N-BASE	15	5/2/2017 7:55:00 AM	Very fine to fine grain sand, trace fine to coarse gravel	5YR 4/6, yellowish red	Moist, no odor	3.9	8.51	1990	320	<20.9	2810
P-7N-TOP	2	5/2/2017 7:30:00 AM	Fine grain sand with gravel and cobbles, some fines	5YR 4/6 as base with pockets of 10YR6/8, brownish yellow	Very moist, no odor	5.2	9.39	1830	<106	<106	<212
P-3S-BASE	12	5/2/2017 10:45:00 AM	Slightly plastic and soft silty clay, trace sand and gravel	10YR 4/4, dark yellowish brown and 10YR 4/2, dark grayish brown	Moist, slight chemical odor	22.8	4.60	654	1800	<25.9	1930
P-9S-TOP	2	5/2/2017 11:40:00 AM	Same sand as previous samples with soft, slightly plastic clay	10YR 4/3, brown	Moist, slight chemical odor	19.2	6.47	504	2050	186	1590

The pH of the samples collected from the soil/fill near the north abutment ranged from 8.51 to 9.39. These ranges are characterized by the National Bureau of Standards Circular 579 as a strongly to very strongly alkaline environment [41]. The south abutment's soil samples had a pH range of 4.60 to 6.47, which would be classified as a very strongly acid to slightly acid environment. For steel, where corrosion is controlled by oxygen reduction, the corrosion rate is independent of pH where pH is greater than 4 and less than 10. Soil resistivity of the samples collected from the soil/fill materials on the north abutment ranged from 1,830 ohms-cm to 1,990 ohms-cm, and from 504 ohms-cm to 654 ohms-cm near the south abutment. Resistivity does not directly correlate to a corrosion rate, but does indicate a relative corrosivity of a soil, with lower resistivity being more corrosive than higher resistivity. Chloride concentrations at the north abutment ranged from non-detect (<106) to 320 mg/kg, and at the south abutment ranged from 1,800 to 2,050 mg/kg. Chloride

concentrations exceeding 250 mg/kg are identified as being of concern for corrosion for buried ferrous materials. The percent moisture of P-9S Top and P-3S-Base were 22.8 and 19.2 percent (respectively), whereas the soil moisture of P-4N-Base and P-7N-Base were 3.9 and 5.2 percent (respectively). Sulfate concentrations were non-detect with a range of < 20.9 to <106 mg/kg at the north abutment, and a range of non-detect (<25.9) to 186 mg/kg near the south abutment. The Federal Highway Administration (FHWA) classifies sulfate concentrations greater than 200 ppm as being aggressive. Table B3 shows the maximum corrosion rate and soil properties from some other studies.

Table B3. Summary of maximum corrosion rate, length of exposure, and soil properties from other studies.

Corrosion rate (μm/year)	Years exposed	pH	Resistivity (Ω cm)	Chloride (ppm)	Source
18	22	5.1–6.0	50,000–70,000	16–59	Wong and Law 1999
30	20	Not given	Not given	Not given	Manning and Morley 1981
15	12	Not given	Not given	Not given	Manning and Morley 1981
30	46	Not given	Not given	Not given	Manning and Morley 1981
58.9	6.8	Not given	Not given	Not given	Escalante 1992
25.6	6.8	7	1,170	Not given	Escalante 1992
12.9	12.9	7.7	2,080	Not given	Escalante 1992
43.6	2.8	7	1,170	Not given	Escalante 1992
47.8	2.8	7.2	455	Not given	Escalante 1992
37.8	6.8	7.4	710	Not given	Escalante 1992
16.5	12.9	7.4	710	Not given	Escalante 1992
17.5	2.8	Not given	Not given	Not given	Escalante 1992
14	12.9	Not given	Not given	Not given	Escalante 1992
58	4.5	Not given	Not given	Not given	Ohsaki 1982
47.6	7	7.4–8.2	850–7,000	0.3	Romanoff 1962
20.7	23	Not given	Not given	Not given	Romanoff 1962
82.3	11	6.9	4,300–11,000	0.6	Romanoff 1962
47.6	11	8.1	800–1,290	0.5	Romanoff 1962
34.6	11	Not given	950–1,610	0	Romanoff 1962
15.9	12	7.7–8.4	345–1,300	0.5	Romanoff 1962
19	34	8.2	300,000	17.8	This study
13.3	35	7.7	150,000	256	This study
15.3	38	7.5	150,000	444	This study

In summary, there are many factors that could potentially lead to the corrosion of steel substructure in subsurface environments. Some of these include soil composition, pH, soil resistivity, moisture content, oxygen levels, and fluctuating groundwater table. Groundwater was not encountered during the excavation and the results from the soil/fill from the north abutment

did not show a particularly corrosive environment in terms of pH and soil resistivity. However, as indicated by the visual inspection of the H-piles and the presence of tubercles, significant corrosion was occurring on many of the steel surfaces. In regard to the south abutment, the soil resistivity and chloride concentrations in addition to the higher number of bacteria colonies found would most likely contribute to the severe corrosion observed.

B3. Corrosion of Steel H-Piles in Decomposed Granite in Singapore

To study the corrosion of steel H-piles in a completely decomposed granite, piles were exposed by excavation 22 years after their installation. The ground was overlain with 1.0–1.5 m of fill material followed by completely decomposed granite. The decomposed granite was completely soil-like in consistency, with all the minerals, except quartz, in the original granite having been altered into clay minerals or clay or silt particles. The properties of the decomposed granite are summarized as follows:

- Liquid limit = 52–55%
- Plasticity index = 19–25%
- Natural water content = 33–41%
- Sand particle content = 36–45%
- Silt sized particle content = 21–29%
- Clay sized particle content = 32–36%

Chemical tests were performed on ground-water samples collected from two water standpipe wells near Piers 1 and 2. The test results are as shown in the Table B4. No resistivity tests were

conducted at the project site, but tests done in the same decomposed granite in nearby areas indicated resistivity values in the range of 500–700 ohm/m.

Table B4. Results of chemical tests on ground water.

Tests (mg/l) (1)	Results	
	Well 1 (2)	Well 2 (3)
Cations		
Sodium (Na)	20	36
Potassium (K)	7.3	12
Calcium (Ca)	59	34
Ammonium (NH_4)	0.1	0.1
Hydrogen (H)	1.0×10^{-6}	7.9×10^{-6}
Anions		
Chloride (Cl)	16	59
Sulfate (SO_4)	46	108
Nitrate (NO_3)	2.7	1.5
Bicarbonate (HCO_3)	246	54
Hydroxyl (OH)	1.0×10^{-8}	1.3×10^{-9}
pH Value	6.0	5.1
Free carbon dioxide	79	243
Total alkalinity (as $CaCO_3$)	202	44
Total dissolved solids	62,320	2,490

It was observed that a uniform roughening of the surfaces of the piles had occurred since their installation. Generalized attack of the pile material due to corrosion was evident, but no pitting was observed. A total of nine existing H−piles was surveyed. The wall thickness of these piles at reduced levels of 102.35 and 99.75m of the excavated site was measured. There was a total of 11 measuring points at RL 102.35m and 48 measuring points at RL 99.75m. The measured data are shown in Table B5. The corrosion rate was estimated using a nominal original wall thickness of 12.83 mm. The estimated average and maximum corrosion rates for each pile are shown in Table B6. The overall average estimated corrosion rates and their standard deviations are shown in Table B7. From Table B7, it is seen that the corrosion rate was estimated to be 0.011 mm/year, both above and below the water table. Table B6 indicates that the maximum corrosion was 0.015 mm/year at RL 99.75m and 0.018/year at RL 102.35m. As stated earlier, the water table was at RL101.6m.

Table B5. Measured wall thickness and estimated corrosion rates.

Reduced level (m) (1)	Pier number (2)	Pile number (3)	Measured wall thickness (mm) (4)	Estimated loss of wall thickness (mm) (5)	Estimated corrosion rate over 22 years (mm/year) (6)
99.75	1	1	12.37	0.46	0.0105
99.75	1	1	12.28	0.55	0.0125
99.75	1	1	12.28	0.55	0.0125
99.75	1	2	12.39	0.44	0.0100
99.75	1	2	12.28	0.55	0.0125
99.75	1	2	12.20	0.63	0.0143
99.75	1	3	12.33	0.50	0.0114
99.75	1	3	12.44	0.39	0.0089
99.75	1	3	12.36	0.47	0.0107
99.75	1	3	12.26	0.57	0.013
99.75	1	3	12.32	0.51	0.0116
99.75	1	3	12.28	0.55	0.0125
99.75	1	3	12.23	0.60	0.0136
99.75	1	3	12.21	0.62	0.0141
99.75	1	3	12.30	0.53	0.0120
99.75	1	4	12.19	0.64	0.0145
99.75	1	4	12.30	0.53	0.0120
99.75	1	4	12.27	0.56	0.0127
99.75	1	4	12.25	0.58	0.0132
99.75	1	5	12.36	0.47	0.0107
99.75	1	5	12.30	0.53	0.0120
99.75	1	5	12.50	0.33	0.0075
99.75	1	5	12.39	0.44	0.0100
99.75	1	5	12.30	0.53	0.0120
99.75	1	5	12.35	0.48	0.0109
99.75	1	5	12.37	0.46	0.0105
99.75	1	5	12.35	0.48	0.0109
99.75	1	5	12.21	0.62	0.0141
99.75	1	6	12.44	0.39	0.0089
99.75	1	6	12.30	0.53	0.0120
99.75	1	6	12.31	0.52	0.0118
99.75	1	6	12.36	0.47	0.0107
99.75	1	6	12.36	0.47	0.0107
99.75	1	6	12.40	0.43	0.0098
99.75	1	6	12.50	0.33	0.0075
99.75	1	6	12.48	0.35	0.0080
99.75	1	7	12.31	0.52	0.0118
99.75	1	7	12.46	0.37	0.0084
99.75	1	7	12.30	0.53	0.0120
99.75	1	7	12.38	0.45	0.0102
99.75	1	7	12.36	0.47	0.0107
99.75	1	7	12.46	0.37	0.0084
99.75	1	7	12.40	0.43	0.0098
99.75	1	8	12.46	0.37	0.0084
99.75	1	8	12.40	0.43	0.0098
99.75	1	8	12.55	0.28	0.0064
99.75	1	8	12.46	0.37	0.0084
99.75	1	8	12.38	0.45	0.0102
102.35	1	6	12.64	0.19	0.0043
102.35	1	6	12.64	0.19	0.0043
102.35	1	7	12.24	0.59	0.0134
102.35	1	7	12.15	0.68	0.0155
102.35	1	7	12.27	0.56	0.0127
102.35	1	8	12.04	0.79	0.0180
102.35	1	8	12.16	0.67	0.0152
102.35	2	2	12.44	0.39	0.0089
102.35	2	2	12.44	0.39	0.0089
102.35	2	2	12.45	0.38	0.0086
102.35	2	2	12.50	0.33	0.0075

Table B6. Estimated Average and Maximum Corrosion Rates for Each Pile.

Reduced level (m) (1)	Pile number (2)	Pier number (3)	Average corrosion rate (mm/year) (4)	Maximum corrosion rate (mm/year) (5)
102.35	2	2	0.008	0.009
102.35	6	1	0.004	0.004
102.35	7	1	0.014	0.015
102.35	8	1	0.017	0.018
99.75	1	1	0.012	0.013
99.75	2	1	0.012	0.014
99.75	3	1	0.012	0.014
99.75	4	1	0.013	0.015
99.75	5	1	0.011	0.014
99.75	6	1	0.010	0.012
99.75	7	1	0.010	0.012
99.75	8	1	0.009	0.010

Table B7. Estimated overall corrosion rates and standard deviations.

Reduced level (m) (1)	Number of piles (2)	Total number of measuring points (3)	Estimated overall average corrosion rates (mm/year) (4)	Standard deviations of estimated corrosion rates (mm/year) (5)
102.35	4	11	0.0107	0.0046
99.75	9	48	0.0109	0.0019

In summary, the estimated average corrosion rate is 0.01 mm/year and the estimated maximum corrosion rate of 0.015–0.018 mm/year for the steel H piles exposed after 22 years in the ground. The sulfate content, chloride content, and the pH values of the ground water in the soil are not within the critical range stipulated by the FHWA standards. The low estimated average corrosion rates indicate that the FHWA standards are applicable for estimating cases where steel piles are safe from corrosion. The findings by Romanoff indicated that in undisturbed natural soils the corrosion rate of steel piles driven into such soils is very small are valid also for the completely decomposed granite of Singapore. A high annual temperature in the range of 25–35°C is not a factor that would influence the rate of corrosion for steel piles installed in the decomposed granite.

B4. Measuring the Underground Corrosion of Steel Piling at Turcot Yard, Montreal, Canada-A 14-year study

Construction of the Trans Canadian Highway at the Turcot Yard interchange, Montreal, and concern about the corrosivity of the soil in that area, resulted in a long-term program to study the corrosion of steel H-piles at that site. Three sets of steel H-piles were placed in the ground, one set without protection, a second set coated in the disturbed soil region, and a third set with concrete caps. The soil properties are given in Tables B8 and B9.

Table B8. Soil properties as a function of distance from the soil surface at Sites A.

Site A Soil Samples	Depth ft	Soil Type	Resistivity Ω-cm	pH
1	3 - 4.5	Fill	2030	7.8
2	5 - 6.5	Fill	2130	7.6
3	6.5 - 8	Boulder	-	-
4	8 - 9.5	Shale	-	-
5	9.5 - 10	Peat	1170	7.0
6	10 - 10.5	Peat	-	-
7	10.5 - 11.5	Marle	1630	7.4
8	11.5 - 13	Marle	1880	7.3
9	13 - 13.9	Clay	1470	7.2
10	13.9 - 14.5	Silt-Gravel	-	-
11	15 - 15.9	Silt-Gravel	4570	8.2
12	15.9	Boulder	-	-

Note: Multiply ft by 0.3 to obtain m.

Table B9. Soil properties as a function of distance from the soil surface at Site B.

Site B Soil Samples	Depth ft	Soil Type	Resistivity Ω-cm	pH
1	2 - 3.5	Fill	510	7,2
2	3.5 - 5	Fill	400	7.2
3	5 - 6.5	Fill	1020	7.5
4	7 - 8.5	Fill	1220	6.9
5	8.5 - 10	Peat	-	-
6	10 - 11.5	Peat	-	-
7	11.5 - 12	Marle	460	6.8
8	12 - 13.5	Marle	600	7.3
9	13.5 - 14.5	Clay	1120	7.1
10	14.5 - 15	Silt-Gravel	-	-
11	15 - 16.5	Silt-Gravel	4570	7.8
12	16.5 - 18	Gravel	-	-
13	18 - 20	Silt-Sand	-	-
14	20 - 21.5	Silt-Sand	4830	7.7
15	22	Silt	-	-

Note: Multiply ft by 0.3 to obtain m.

Table B10 reveals the corrosion rate calculated from these data and the corrosion current density for the piles that remain in the ground. As can be seen, the average corrosion rate in every case was less than 1 mpy (25.4 µm/y). The pH was near neutral or slightly alkaline in all cases and was not considered a source of corrosion problems to steel. The soil resistivity at Site A varied between 1170 Ω-cm and 4570 Ω-cm, and past experience suggested that it was not an aggressive soil. In general, the same was true at site B, except for sections with a soil resistivity below 600 Ω-cm, where soil conditions could be corrosive to steel.

Table B10. Summary of electrochemical data.

Pile ID	Average Corrosion Current Density mA/sq ft	Number of Corrosion Current Measurements over 14 y	Exposure Time* years	Average Corrosion Rate From Corrosion Current* mils/yr (µm/y)
A-1	1.12	6	6.8	0.55 (14.0)
A-2	1.05	12		
A-3	0.75	10	12.9	0.37 (9.4)
A-4	0.42	11		
A-5	0.30	2	2.8	0.15 (3.7)
A-6	0.24	2		
A-7	0.40	10		
B-1	1.04	2	2.8	0.51 (13.0)
B-2	1.42	6	6.8	0.70 (17.7)
B-3	1.56	12	12.9	0.77 (19.5)
B-4	1.98	12		
B-5	1.40	12		
B-6	0.88	2		
B-7	1.11	2	2.8	0.55 (13.9)
A-10	0.26	8		
C-1	0.66	2	2.8	0.32 (8.2)
C-2	0.86	12		
C-3	0.92	11	12.9	0.45 (11.5)
C-4	0.51	5	6.8	0.25 (6.4)
C-5	0.94	12		
C-6	0.77	4		
C-7	0.53	10	12.9	0.26 (6.4)

*Note: Missing data indicate that piles are still in place.
Multiply mA/sq ft by 10.76 to obtain mA/sq m.

The piles at site B, coated in the disturbed soil region, on the average showed a higher rate of deterioration than the piles at the other two sites, including the bare piles. This was not unexpected,

since the soil analysis data indicated the soil resistivity at this site was low, <600 Ω-cm in some regions, as revealed in Table B9.

The corrosion current density of real structure which is supported by 32 interconnected steel H-piles was an approximately a factor of 3 less than the corrosion current density for the concrete capped piles. This low corrosion current was probably due to a shielding effect, where the applied polarizing current was only reaching the piles on the outer fringes of the pile cluster. These data suggested that the polarizing current was only polarized between 1/3 to 1/5 of the piles in the cluster.

A summary of the corrosion rate of all the piles in three soil zones calculated from the physical measurements and an average of the total corrosion obtained from these data is listed in Table B11.

Table B11. Average corrosion rate of the extracted piles at three soil levels calculated from physical measurements.

Pile ID	Disturbed Soil Top 4 ft mils/y*	Interface Soil Mid 2 ft mils/y*	Undisturbed Soil Below Mid mils/y*	Overall Average mils/y (µm/y)
A-1	0.72	1.01	0.26	0.42 (10.6)
A-3	0.51	0.07	0.23	0.27 (6.8)
A-5	0.77	1.72	0.11	0.35 (8.9)
B-1	0.80	0.00	0.52	0.53 (10.9)
B-2	0.27	1.49	0.55	0.58 (14.7)
B-3	0.13	0.65	0.55	0.50 (12.8)
B-7	1.88	0.00	0.17	0.43 (10.9)
C-1	0.00	0.69	0.30	0.28 (7.2)
C-3	0.00	0.55	0.34	0.31 (7.9)
C-4	0.00	2.32	0.22	0.33 (8.4)
C-7	0.00	0.41	0.30	0.27 (6.9)
Average		0.81	0.32	0.39 (9.9)

*Note: Multiply mils/y by 25.4 to calculate µm/y.

The corrosion rate calculations in this table were based on the decrease in thickness of the flange that exceeded the standard deviation of the original thickness of the piles. In general, coating the top of the pile in the disturbed soil region was beneficial, but where the coating failed, corrosion attack was severe. The piles of set C were capped with concrete to simulate the actual pier structure, and the effect of the concrete on the corrosion process is especially interesting for this reason. Removal of the concrete cap clearly indicated that the concrete had protected the steel H-pile from any corrosion attack. However, visual examination revealed shallow pitting in the area immediately below the concrete cap. This study also indicates that the electrochemical polarization technique tended to overestimate corrosion rate by approximately 30%, for values greater than 0.25 mpy (6.3 μm/y). The average corrosion rate for the bare piles in the disturbed soil region was 0.67 mpy (16.9 μm/y). In the soil interface region, the average corrosion for all the piles was 0.81 mpy (20.6 μm/y), and in the undisturbed soil region, their average corrosion rate was 0.32 mpy (8.1 μm/y). The average corrosion rate for all the piles over their entire surface was 0.39 mpy (9.9 μm/y).

In summary, electrochemical polarization measurements was useful for evaluating the corrosion of steel H-piles in soil, even though the measurement overestimates the rate of corrosion by approximately 30 percent. This 14-year study revealed that the average corrosion rate of the steel H-piles at Turcot Yard was low in all cases and was especially low in undisturbed soil where the average corrosion rate was less than 0.33 mpy (8.4 μm/y). The electrochemical measurements also showed that the corrosion current of piles supporting a pier decreased by more than an order of magnitude over the 14-year period.

B5. Corrosion of Steel Abutment Piles in IOWA Bridges

In 2006, Iowa DOT requested to examine and document the condition of steel abutment piles at twelve highway bridges at various locations around the state. In 2008, three additional bridges were included in the study. The purpose of the investigation was to determine the extent to which the steel abutment piles at the selected bridges had deteriorated, and to document the physical conditions at each abutment. The investigation was limited to the upper portions of the piles directly below the abutment footings, where corrosion had been observed at several bridges during previous Iowa DOT inspections.

The investigation showed that the most severe corrosion was observed in piles that were exposed by erosion caused by roadway runoff. These piles exhibited the greatest reduction in cross sectional area and the shortest expected remaining life. Corrosion was significantly more severe at pile segments that were located above the grade line, compared to portions that were covered with soil. High chloride contents, low soil resistivity and extensive section loss were observed at areas exhibiting severe runoff erosion. Areas that exhibited little runoff erosion typically had lower chloride content, higher resistivity, and little section loss. Several of the exposed piles were nearing or had reached a 50 percent reduction in cross sectional area. Average rates of cross-sectional area loss for portions of piles exposed to the atmosphere ranged from approximately 0.3 percent/year to 1.4 percent/year. The most severe section loss corresponded to an average thickness loss rate of approximately 4 mils/year for each face of the pile flanges at the measured cross section. Averaged section loss rates for the excavated below-grade portions of exposed piles ranged from less than 0.1 percent to approximately 0.8 percent/year. Soil-covered piles, even those situated in soils with relatively low resistivity and high chloride content, exhibited little corrosion, presumably due to a

limited supply of oxygen. The expected remaining life of all of the fully soil-covered piles was greater than 50 years. Section loss rates for soil-covered piles were typically less than 0.1 percent/year. Soil pH did not appear to be a factor contributing to the corrosion of any of the examined piles. In addition, the combination of low levels of sulfate content and relatively aerobic conditions indicated by the redox potential (Eh) measurements suggest that microbial-induced corrosion did not play a significant role in determining site corrosivity. Steel free-corrosion potential measurements indicated that all of the piles were subject to some degree of corrosion. The correlation between potential and observed section loss was not as strong, however, as that observed between resistivity and section loss. The greatest factor contributing to corrosion of the examined piles was roadway runoff, causing erosion and exposure to oxygen and introducing moisture and chlorides to the sites. Where piles remained covered with soil, corrosion was observed to occur slowly.

In summary, soil consolidation and erosion caused by roadway runoff have exposed the upper portions of steel piles at the abutments of numerous bridges in Iowa and elsewhere. The exposed portions of the piles were susceptible to accelerated corrosion rates due to the abundance of moisture, oxygen, and chlorides at these locations.

APPENDIX C

USING GRNN MODEL FOR PREDICTING CORROSION IN LEO FRIGO H-PILES

The analytical results of the soil, the corrosion potential, and the observed section loss in Leo Frigo Bridge were used to predict the corrosion behavior of steel using the previously developed and trained GRNN model. Results are shown in Table C1.

Table C1. Soil analytical results, corrosion potential, corrosion current density and the section loss in Leo Frigo Bridge

Pier	Lab Sample ID	Resistivity (ohm-cm)	pH	Chloride (mg/kg)	Sulfate (mg/kg)	Corrosion potential (V)		Section loss (%)		Current density (A/m^2)		Rate (mm/yr)		Rate (mm/yr)
						Measured	Predicted	Observed	Predicted	min	max	min	max	Average
6	TP06SW-03	200	8.2	197	76.8	0.4	-0.31	0-5	30-40	0.01	0.06	11.6	69.6	40.6
6	TP06SW-04	500	7.9	1590	278	0.4	-0.3	0-5	10-20	0.01	0.03	11.6	34.8	23.2
6	TP06SW-06	800	7.9	4860	233	0.4	-0.321	0-5	10-20	0.01	0.08	11.6	92.8	52.2
6	TP06SW-07	1100	8.4	2620	122	0.4	-0.4	0-5	5-10	0.01	0.05	11.6	58	34.8
10	TP10S-1	470	8.2	510	44.8	-	-0.04	0-5	20-30	0.01	0.03	11.6	34.8	23.2
10	TP10S-2	600	7.8	236	54.8	-	-0.025	0-5	0-5	0.01	0.02	11.6	23.2	17.4
11	TP11S-1	220	7.9	601	30.9	-	-0.03	0-5	0-5	0.02	0.05	23.2	58	40.6
11	TP11S-2	800	7.8	264	37.3	-	-0.03	0-5	5-10	0.02		23.2		23.2
12	TP12S-1	160	8.3	670	543	-	-0.019	5-10	10-20	0.04	0.05	46.4	58	52.2
13	TP13NE-1	300	9	560	409	0.37	-0.318	5-10	10-20	0.03	0.05	34.8	58	46.4
13	TP13NE-2	1200	7.7	1400	646	0.37	-0.24	5-10	5-10	0.03	0.06	34.8	69.6	52.2
13	TP13NE-3	1600	7.9	281	50.9	0.37	-0.218	5-10	0-5	0.03	0.06	34.8	69.6	52.2
13	TP13NE-4	1300	8	5370	286	0.37	-0.244	5-10	5-10	0.04	0.08	46.4	92.8	69.6
13	TP13NE-5	300	8.1	1870	1600	0.37	-0.241	5-10	5-10	0.04	0.05	46.4	58	52.2
13	TP13NE-6	410	7.4	268	51.8	0.37	-0.233	5-10	0-5	0.03	0.05	34.8	58	46.4
13	TP13NE-7	530	8.1	277	29.6	0.37	-0.219	5-10	0-5	0.04	0.06	46.4	69.6	58
13	TP13S-1	410	7.9	125	26.7	0.37	0.222	5-10	0-5	0.04	0.06	46.4	69.6	58
13	TP13S-2	800	7.8	1320	484	0.37	-0.297	5-10	10-20	0.03	0.05	34.8	58	46.4
13	TP13S-3	430	8.1	1050	176	0.37	-0.319	5-10	10-20	0.03	0.05	34.8	58	46.4
13	TP13SE-01	210	7.9	1590	145	0.37	-0.361	5-10	20-30	0.04	0.07	46.4	81.2	63.8
13	TP13SE-05	1300	8.9	1550	101	0.37	-0.24	5-10	5-10	0.04	0.06	46.4	69.6	58
14	TP14S-1	700	8.3	1800	138	-	-0.097	5-10	10-20	0.04	0.05	46.4	58	52.2

14	TP14S-2	800	8	1430	923	-	-0.16	5-10	10-20	0.03	0.04	34.8	46.4	40.6
14	TP14S-3	1500	7.6	3080	2330	-	-0.04	5-10	5-10	0.04	0.06	46.4	69.6	58
15	TP15S-2	1300	8	296	121	-	-0.033	0-5	5-10	0.02	0.03	23.2	34.8	29
15	TP15S-3	1100	8.2	298	174	-	-0.032	0-5	5-10	0.01	0.02	11.6	23.2	17.4
16	TP16SE-1	900	8.1	381	4303	-	0.052	0-5	>40	0.04	0.05	46.4	58	52.2
16	TP16SE-2	800	8	896	396	-	-0.082	0-5	10-20	0.03	0.05	34.8	58	46.4
16	TP16SE-3	800	7.8	140	27.3	-	-0.025	0-5	5-10	0.01	0.02	11.6	23.2	17.4
16	TP16SE-4	800	8.1	259	214	-	-0.1	0-5	10-20	0.01	0.02	11.6	23.2	17.4
17	TP17S-1	440	8.3	430	26.9	-	0.035	0-5	5-10	0.02	0.05	23.2	58	40.6
17	TP17S-2	900	8	259	27.7	-	-0.03	0-5	5-10	0.02	0.03	23.2	34.8	29
17	TP17S-3	700	8.1	---	291	-	-0.08	0-5	10-20	0.03		34.8		34.8
18	TP18SE-1	1400	8	---	123	-	-0.031	0-5	5-10	0.01		11.6		11.6
18	TP18SE-2	800	8.9	222	518	-	-0.1	0-5	10-20	0.02	0.03	23.2	34.8	29
18	TP18SE-3	1700	8.1	1230	319	-	-0.042	0-5	5-10	0.01	0.05	11.6	58	34.8
19	TP19NE-1	900	8.1	1980	81	0.3	-0.285	0-5	10-20	0.02	0.04	23.2	46.4	34.8
19	TP19NE-2	570	7.9	391	149	0.3	-0.292	0-5	10-20	0.03	0.08	34.8	92.8	63.8
19	TP19NE-3	460	7.8	2130	97.8	0.3	-0.32	0-5	10-20	0.05	0.06	58	69.6	63.8
19	TP19NE-4	1200	7.9	1590	176	0.3	-0.24	0-5	5-10	0.01	0.05	11.6	58	34.8
19	TP19NW-1	700	8.1	175	27.1	0.3	-0.22	0-5	0-5	0.01	0.05	11.6	58	34.8
19	TP19NW-2	1100	7.6	607	215	0.3	-0.23	0-5	5-10	0.01	0.06	11.6	69.6	40.6
19	TP19S-1	700	7.7	283	268	0.3	-0.3	0-5	10-20	0.02	0.07	23.2	81.2	52.2
19	TP19S-3	700	7.9	1740	32.3	0.3	-0.23	0-5	0-5	0.05	0.07	58	81.2	69.6
19	TP19S-4	1500	8	4060	38.6	0.3	-0.24	0-5	10-20	0.01	0.08	11.6	92.8	52.2
19	TP19S-5	900	7.6	287	54.9	0.3	-0.23	0-5	5-10	0.02	0.05	23.2	58	40.6
19	TP19SW-01	1100	8.4	258	357	0.3	-0.23	0-5	5-10	0.01	0.02	11.6	23.2	17.4
19	TP19SW-02	1100	8.4	183	76.2	0.3	-0.222	0-5	5-10	0.01		11.6		11.6
20	TP20S-1	410	8.2	104	117	-	-0.19	0-5	20-30	0.01	0.03	11.6	34.8	23.2
20	TP20S-3	700	7.4	2250	249	-	-0.09	0-5	10-20	0.03	0.04	34.8	46.4	40.6
20	TP20S-4	340	8.1	7280	62.4	-	-0.11	0-5	0-5	0.04	0.05	46.4	58	52.2
20	TP20S-5	410	8	2510	462	-	-0.12	0-5	10-20	0.04	0.06	46.4	69.6	58
21	TP21NW-1	370	7.8	1760	161	-	-0.12	20-30	10-20	0.04	0.06	46.4	69.6	58
21	TP21S-1	400	8.4	1890	87.7	-	-0.12	20-30	10-20	0.05		58		58
21	TP21S-2	410	8.4	463	79.2	-	-0.12	20-30	10-20	0.04	0.05	46.4	58	52.2
21	TP21S-3	250	8.1	1220	263	-	-0.12	20-30	10-20	0.05		58		58
21	TP21S-4	380	8	3970	21800	-	-0.12	20-30	>40	0.06	0.07	69.6	81.2	75.4
22	TP22N-1	310	8.1	866	5760	-	-0.13	>40	>40	0.06	0.08	69.6	92.8	81.2
22	TP22N-2	340	7.9	1130	998	-	-0.164	>40	20-30	0.07	0.09	81.2	104.4	92.8
22	TP22N-3	610	7.6	1920	303	-	-0.118	>40	10-20	0.07	0.09	81.2	104.4	92.8
22	TP22N-4	700	7.7	685	2970	-	-0.08	>40	>40	0.05	0.08	58	92.8	75.4
22	TP22S-1	300	8.1	291	5270	-	-0.08	>40	>40	0.06	0.09	69.6	104.4	87
22	TP22S-2	290	7.7	1720	1660	-	-0.04	>40	5-10	0.04	0.08	46.4	92.8	69.6

22	TP22S-3	260	8.2	1120	33.8	-	-0.05	>40	20-30	0.05	0.09	58	104.4	81.2
22	TP22S-4	5700	8.9	158	3150	-	-0.04	>40	>40	0.05	0.08	58	92.8	75.4
22	TP22SW-1	230	9.1	29.8	5840	-	-0.04	>40	10-20	0.05	0.08	58	92.8	75.4
22	TP22SW-2	700	8	2870	230	-	-0.095	>40	10-20	0.06	0.08	69.6	92.8	81.2
22	TP22SW-3	900	7.9	971	274	-	-0.074	>40	10-20	0.07	0.09	81.2	104.4	92.8
23	TP23S-1	4100	7.8	249	123	-	-0.03	20-30	0-5	0.03	0.05	34.8	58	46.4
23	TP23S-2	270	8.9	229	176	-	-0.15	20-30	20-30	0.04	0.05	46.4	58	52.2
23	TP23S-4	700	8.1	139	109	-	-0.1	20-30	10-20	0.05	0.06	58	69.6	63.8
23	TP23S-5	100	8.3	1150	31.4	-	-0.15	20-30	20-30	0.05	0.06	58	69.6	63.8
23	TP23S-6	450	7.1	6180	67.3	-	-0.16	20-30	10-20	0.06	0.07	69.6	81.2	75.4
24	TP24NW-1	4200	8.5	380	26.9	0.56	-0.542	0-5	0-5	0.01	0.05	11.6	58	34.8
24	TP24NW-3	1700	7.3	3400	67.3	0.56	-0.542	0-5	10-20	0.01	0.06	11.6	69.6	40.6
24	TP24NW-4	1500	7.5	34.2	26.4	0.56	-0.55	0-5	0-5	0.01		11.6		11.6
24	TP24NW-5	1200	8	626	32.8	0.56	-0.53	0-5	5-10	0.01	0.05	11.6	58	34.8
24	TP24S-1	2800	8.1	91	37.4	0.56	-0.525	0-5	0-5	0.01		11.6		11.6
24	TP24S-2	1000	8.3	143	32.3	0.56	-0.524	0-5	5-10	0.01		11.6		11.6
24	TP24S-4	100	7.7	106	81.6	0.56	-0.52	0-5	30-40	0.01	0.08	11.6	92.8	52.2
24	TP24S-5	700	7.8	42.4	130	0.56	-0.532	0-5	>40	0.01	0.05	11.6	58	34.8
24	TP24S-6	1500	7.5	545	217	0.56	-0.532	0-5	5-10	0.01	0.05	11.6	58	34.8
25	TP25NE-1	1300	8.3	2170	70.3	0.282	-0.24	30-40	5-10	0.03	0.07	34.8	81.2	58
25	TP25NE-2	270	8.4	396	158	0.282	-0.219	30-40	10-20	0.03	0.07	34.8	81.2	58
25	TP25NE-3	260	7	159	227	0.282	-0.26	30-40	20-30	0.03	0.07	34.8	81.2	58
25	TP25NE-4	900	7.7	98	662	0.282	-0.27	30-40	20-30	0.04	0.07	46.4	81.2	63.8
25	TP25NE-5	700	8	7710	66.9	0.282	-0.133	30-40	0-5	0.05	0.08	58	92.8	75.4
25	TP25NW-1	550	8	4330	171	0.282	-0.22	30-40	10-20	0.06	0.07	69.6	81.2	75.4
25	TP25S-1	370	7.8	259	1150	0.282	-0.43	30-40	30-40	0.04	0.06	46.4	69.6	58
25	TP25S-2	450	8.2	862	248	0.282	-0.219	30-40	10-20	0.04	0.07	46.4	81.2	63.8
32	TP32NE-1	190	8.1	1410	277	0.31	-0.286	0-5	30-40	0.03	0.04	34.8	46.4	40.6
32	TP32NE-2	160	7.6	3980	664	0.31	-0.295	0-5	10-20	0.02	0.03	23.2	34.8	29
32	TP32NE-3	250	8.1	3780	158	0.31	-0.12	0-5	10-20	0.02	0.05	23.2	58	40.6
32	TP32NE-5	160	8	2610	143	0.31	-0.34	0-5	20-30	0.05	0.05	58	58	58
32	TP32NE-6	3500	7.8	3130	226	0.31	-0.34	0-5	5-10	0.01	0.03	11.6	34.8	23.2
32	TP32NW-02	350	8.5	2640	70.3	0.31	-0.12	0-5	10-20	0.02	0.04	23.2	46.4	34.8
32	TP32NW-08	1000	8	10300	50.9	0.31	-0.345	0-5	10-20	0.01	0.03	11.6	34.8	23.2
39	TP39NW-1	370	8.4	3460	97.7	0.41	-0.312	5-10	10-20	0.02	0.05	23.2	58	40.6
39	TP39NW-2	170	7.8	55	148	0.41	-0.39	5-10	>40	0.02	0.05	23.2	58	40.6
39	TP39NW-3	170	7.6	2570	117	0.41	-0.39	5-10	20-30	0.03	0.04	34.8	46.4	40.6
39	TP39NW-4	80	7.9	1630	46.8	0.41	-0.39	5-10	30-40	0.04	0.05	46.4	58	52.2
39	TP39NW-5	90	8.3	1640	50	0.41	-0.39	5-10	30-40	0.04	0.05	46.4	58	52.2
39	TP39SE-1	300	7.6	118	322	0.41	-0.51	5-10	20-30	0.01	0.03	11.6	34.8	23.2
39	TP39SE-2	200	8	258	278	0.41	-0.395	5-10	30-40	0.01	0.06	11.6	69.6	40.6

39	TP39SE-3	170	7.9	1110	218	0.41	-0.38	5-10	10-20	0.03	0.04	34.8	46.4	40.6
39	TP39SE-4	1500	7.5	2890	333	0.41	-0.39	5-10	5-10	0.01	0.06	11.6	69.6	40.6
39	TP39SW-03	620	7.9	3170	184	0.41	-0.472	5-10	10-20	0.02	0.05	23.2	58	40.6
39	TP39SW-06	230	8	7850	1140	0.41	-0.394	5-10	5-10	0.04	0.06	46.4	69.6	58
39	TP39SW-07	320	8.5	3730	140	0.41	-0.472	5-10	10-20	0.03	0.05	34.8	58	46.4
39	TP39SW-08	470	8	1150	226	0.41	-0.47	5-10	10-20	0.03	0.05	34.8	58	46.4
43	TP43NE-1	310	8.2	1590	70.2	0.17	-0.12	0-5	10-20	0.03	0.05	34.8	58	46.4
43	TP43NE-2	390	8	11400	2520	0.17	-0.144	0-5	5-10	0.02	0.03	23.2	34.8	29
43	TP43NE-3	350	7.8	266	105	0.17	-0.144	0-5	10-20	0.01	0.03	11.6	34.8	23.2
43	TP43NE-4	900	8.1	1820	30.8	0.17	-0.134	0-5	5-10	0.03	0.06	34.8	69.6	52.2
43	TP43NE-5	800	8.1	1080	169	0.17	-0.175	0-5	10-20	0.02	0.06	23.2	69.6	46.4
44	TP44NW-02	800	7.9	1050	160	-	-0.075	0-5	10-20	0.03	0.04	34.8	46.4	40.6
44	TP44NW-03	1000	8	2410	199	-	-0.035	0-5	5-10	0.01	0.03	11.6	34.8	23.2
44	TP44NW-04	1500	8.2	2010	875	-	-0.04	0-5	5-10	0.01	0.03	11.6	34.8	23.2
44	TP44NW-05	1600	8.2	2050	52.6	-	-0.042	0-5	0-5	0.01	0.03	11.6	34.8	23.2
50	TP50SE-02	570	8.4	960	40.2	-	-0.017	0-5	0-5	0.01	0.03	11.6	34.8	23.2
50	TP50SE-03	200	8.3	1190	27.9	0.18	-0.143	0-5	5-10	0.02	0.03	23.2	34.8	29
50	TP50SE-04	1100	8.2	1130	27	0.18	-0.13	0-5	5-10	0.02	0.03	23.2	34.8	29
50	TP50SE-06	1700	8.2	443	1850	0.18	-0.144	0-5	5-10	0.02	0.04	23.2	46.4	34.8

For better comparison, the average predicted corrosion potential values was plotted against the measured values and the results are shown in Figure C1.

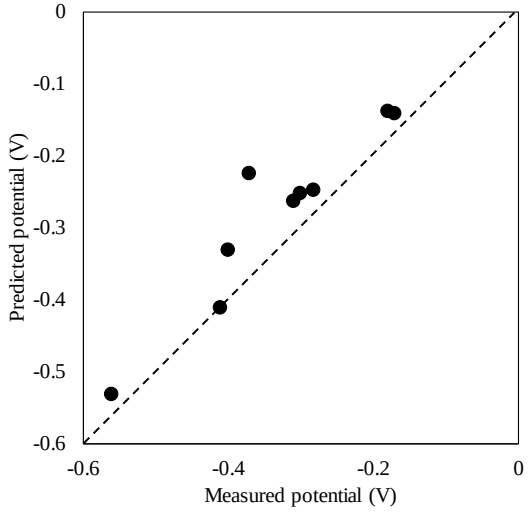

Figure C1. Predicted vs measured corrosion potential values for different piers in Leo Frigo Bridge

As can be seen, a good correlation exists between the measured and predicted corrosion potential values. The observed percentage section loss was reported for different piers of the Leo Frigo Bridge. Our model on the other hand predicts the corrosion current density values. While side by side comparison is not possible, the piers were ranked based on their average predicted corrosion rates and the observed percentage section loss and results are shown in Table C2. The corrosion predicted current densities are converted to the corrosion rate (mm/year) and given in Table C2.

Table C2. Ranked observed section loss and the average predicted corrosion rates

Pier	Observe section loss (%)	Pier	Corrosion rate (mm/year)
22	>40	22	82
25	30-40	25	64
21	20-30	21	60
23	20-30	23	60
12	5-10	13	54
13	5-10	12	52
14	5-10	14	50
39	5-10	20	43
6	0-5	39	43
10	0-5	19	43
11	0-5	43	39
15	0-5	6	38
16	0-5	32	36
17	0-5	17	35
18	0-5	16	33
19	0-5	11	32
20	0-5	24	30
24	0-5	50	29
32	0-5	44	27
43	0-5	18	25
44	0-5	15	23
50	0-5	10	20

According to the FHWA Manual on design and construction of driven pile foundations, 0.08 mm/year for piles buried in fill or disturbed natural soil is consider active corrosion. Thus, based on this simulation, steel piles in all locations, were actively corroding. In addition, the ranking of the predicted corrosion rates match well with the actual observed section loss.

References:

1. Becker, S. and Rudat, K., *I-43 Leo Frigo Memorial Bridge Investigation Report -Draft Executive Summary.* 2014(Wisconsin Department of Transportation).
2. Halim, A., Watkin, E., and Gubner, R., *Short term corrosion monitoring of carbon steel by bio-competitive exclusion of thermophilic sulphate reducing bacteria and nitrate reducing bacteria.* Electrochimica Acta, 2012. **77**: p. 348-362.
3. Ding, L. and Poursaee, A., *The impact of sandblasting as a surface modification method on the corrosion behavior of steels in simulated concrete pore solution.* Construction and Building Materials, 2017. **157**: p. 591-599.
4. Wang, X., Qi, X., Lin, Z., Wang, J., and Gong, N., *Electrochemical Characterization of the Soils Surrounding Buried or Embedded Steel Elements*, in *Pipelines* 2016. p. 110-116.
5. Wong, I.H. and Law, K.H., *Corrosion of steel H piles in decomposed granite.* Journal of geotechnical and geoenvironmental engineering, 1999. **125**(6): p. 529-532.
6. Wong, I., *Methods of resisting hydrostatic uplift in substructures.* Tunnelling and Underground Space Technology, 2001. **16**(2): p. 77-86.
7. Fleming, K., Weltman, A., Randolph, M., and Elson, K., *Piling engineering*2008: CRC press.
8. Benmoussat, A. and Hadjel, M., *Corrosion behavior of low carbon line pipe steel in soil environment.* J Corros Sci Eng, 2005. **7**: p. 14.
9. Fontana, M.G., *Corrosion engineering*2005: Tata McGraw-Hill Education.
10. Wang, H., Sweikart, M.A., and Turner, J.A., *Stainless steel as bipolar plate material for polymer electrolyte membrane fuel cells.* Journal of Power Sources, 2003. **115**(2): p. 243-251.

11. Reiser, C.A., Bregoli, L., Patterson, T.W., Jung, S.Y., Yang, J.D., Perry, M.L., and Jarvi, T.D., *A reverse-current decay mechanism for fuel cells.* Electrochemical and Solid-State Letters, 2005. **8**(6): p. A273-A276.

12. Bentur, A., Berke, N., and Diamond, S., *Steel corrosion in concrete: fundamentals and civil engineering practice*1997: CRC Press.

13. Poursaee, A., *Corrosion measurement techniques in steel reinforced concrete.* Journal of ASTM International, 2011. **8**(5): p. 1-15.

14. Ricker, R.E., *Analysis of pipeline steel corrosion data from NBS (NIST) studies conducted between 1922–1940 and relevance to pipeline management.* Journal of research of the National Institute of Standards and Technology, 2010. **115**(5): p. 373.

15. Yan, M., Sun, C., Xu, J., Dong, J., and Ke, W., *Role of Fe oxides in corrosion of pipeline steel in a red clay soil.* Corrosion Science, 2014. **80**: p. 309-317.

16. Chatterjee, A., Lal, R., Wielopolski, L., Martin, M.Z., and Ebinger, M., *Evaluation of different soil carbon determination methods.* Critical Reviews in Plant Science, 2009. **28**(3): p. 164-178.

17. Ferreira, C.A.M., Ponciano, J.A., Vaitsman, D.S., and Pérez, D.V., *Evaluation of the corrosivity of the soil through its chemical composition.* Science of the total environment, 2007. **388**(1): p. 250-255.

18. Ferreira, C. and Ponciano, J., *Determination of the soil corrosivity of samples from southeastern Brazilian region.* Eurocorr, Maastricht, Holland, 2006.

19. Oldeman, L., Hakkeling, R.u., and Sombroek, W.G., *World map of the status of human-induced soil degradation: an explanatory note*1990: International Soil Reference and Information Centre.

20. Saji, G. *Radiation induced 'long-cell'(macrocell) corrosion in water-cooled reactors of Russian design*. in *Material issues in design, manufacturing and operation of nuclear power plants equipment. In: 11th Prometey Int. Conf., St. Petersburg, Russia*. 2010.

21. Cole, I. and Marney, D., *The science of pipe corrosion: A review of the literature on the corrosion of ferrous metals in soils.* Corrosion science, 2012. **56**: p. 5-16.

22. Wang, X., Qi, X., Lin, Z., Wang, J., and Gong, N., *Electrochemical Characterization of the Soils Surrounding Buried or Embedded Steel Elements*, in *Pipelines 2016*. p. 110-116.

23. Pritchard, O., Hallett, S.H., and Farewell, T.S., *Soil corrosivity in the UK–Impacts on Critical Infrastructure.* Infrastructure Transitions Research Consortium Working paper series, 2013: p. 1-55.

24. Fonseca, I., Niculita, E., Ornelas, I., Carvalho, M., and Vaz, P., *Validation of the Steinrath Index Predictions for the Degree of Soil Aggressiveness Toward Copper Corrosion in Soils Contaminated with Chlorides.* Corrosion, 2015. **71**(10): p. 1267-1277.

25. Beben, D., *Backfill Corrosivity around Corrugated Steel Plate Culverts.* Journal of Performance of Constructed Facilities, 2014. **29**(6): p. 04014159.

26. Decker, J.B., Rollins, K.M., and Ellsworth, J.C., *Corrosion rate evaluation and prediction for piles based on long-term field performance.* Journal of geotechnical and geoenvironmental engineering, 2008. **134**(3): p. 341-351.

27. Trungesvik, K., *Investigations of corrosion rates on steel piles in Norwegian marine sediments*1976: Norwegian Geotechnical Institute.

28. Chaker, V., *Effects of soil characteristics on corrosion*. Vol. 1013. 1989: ASTM International.

29. Liu, T., Wu, Y., Luo, S., and Sun, C., *Effect of soil compositions on the electrochemical corrosion behavior of carbon steel in simulated soil solution. Einfluss der Erdbodenzusammensetzung auf das elektrochemische Verhalten von Kohlenstoffstählen in simulierten Erdbodenlösungen.* Materialwissenschaft und Werkstofftechnik, 2010. **41**(4): p. 228-233.

30. Moore, T. and Hallmark, C., *Soil Properties Influencing Corrosion of Steel in Texas Soils 1.* Soil science society of America journal, 1987. **51**(5): p. 1250-1256.

31. Denison, I. and Hobbs, R., *Corrosion of ferrous metals in acid soils.* J. Res., National Bureau of Standards, 1934. **13**: p. 125.

32. Robinson, W., *Testing soil for corrosiveness.* Materials Performance;(United States), 1993. **32**(4).

33. Fitzgerald, J., *Evaluating soil corrosivity--Then and now.* Materials Performance;(United States), 1993. **32**(10).

34. Peabody, A.W., *Control of pipeline corrosion*1967: National Association of corrosion engineers Houston, Texas.

35. Roberge, P.R., *Handbook of corrosion engineering*2000: McGraw-Hill.

36. Penhale, H., *Corrosion of mild steel plates in some New Zealand soils, after 20 years.* New Zealand journal of science, 1984.

37. Rajani, B. and Makar, J., *A methodology to estimate remaining service life of grey cast iron water mains.* Canadian Journal of Civil Engineering, 2000. **27**(6): p. 1259-1272.

38. Doyle, G., Seica, M.V., and Grabinsky, M.W., *The role of soil in the external corrosion of cast iron water mains in Toronto, Canada.* Canadian geotechnical journal, 2003. **40**(2): p. 225-236.

39. Elias, V. and Christopher, B.R., *Mechanically stabilized earthwalls and reinforced soil slopes, design and construction guidelines,* 1997, Federal Highway Administration: Washington DC.

40. Neville, A.M., *Properties of Concrete*. 4rd ed1995, New York, N. Y.: Longman Scientific & Technical.

41. Gupta, S. and Gupta, B., *The critical soil moisture content in the underground corrosion of mild steel.* Corrosion science, 1979. **19**(3): p. 171-178.

42. Noor, E.A. and Al-Moubaraki, A.H., *Influence of soil moisture content on the corrosion behavior of X60 steel in different soils.* Arabian Journal for Science and Engineering, 2014. **39**(7): p. 5421-5435.

43. Costerton, J.W., Cheng, K., Geesey, G.G., Ladd, T.I., Nickel, J.C., Dasgupta, M., and Marrie, T.J., *Bacterial biofilms in nature and disease.* Annual Reviews in Microbiology, 1987. **41**(1): p. 435-464.

44. Hubert, C., Nemati, M., Jenneman, G., and Voordouw, G., *Corrosion risk associated with microbial souring control using nitrate or nitrite.* Applied microbiology and biotechnology, 2005. **68**(2): p. 272-282.

45. Enning, D., Venzlaff, H., Garrelfs, J., Dinh, H.T., Meyer, V., Mayrhofer, K., Hassel, A.W., Stratmann, M., and Widdel, F., *Marine sulfate-reducing bacteria cause serious corrosion of iron under electroconductive biogenic mineral crust.* Environmental microbiology, 2012. **14**(7): p. 1772-1787.

46. Hamilton, W.A., *Sulphate-reducing bacteria and anaerobic corrosion.* Annual Reviews in Microbiology, 1985. **39**(1): p. 195-217.

47. Little, B.B., Ray, R.I., and Pope, R.K., *The Relationship Between Corrosion and the Biological Sulfur Cycle*, 2000, NAVAL RESEARCH LAB STENNIS SPACE CENTER MS OCEANOGRAPHY DIV.

48. Javaherdashti, R., *A review of some characteristics of MIC caused by sulfate-reducing bacteria: past, present and future.* Anti-corrosion methods and materials, 1999. **46**(3): p. 173-180.

49. Javaherdashti, R., *Impact of sulphate-reducing bacteria on the performance of engineering materials.* Applied microbiology and biotechnology, 2011. **91**(6): p. 1507.

50. Sungur, E.I., TÜRETGEN, İ., Javaherdashti, R., and ÇOTUK, A., *Monitoring and disinfection of biofilm-associated sulfate reducing bacteria on different substrata in a simulated recirculating cooling tower system.* Turkish Journal of Biology, 2010. **34**(4): p. 389-397.

51. Sand, W., *Microbial mechanisms of deterioration of inorganic substrates—a general mechanistic overview.* International Biodeterioration & Biodegradation, 1997. **40**(2-4): p. 183-190.

52. Setareh, M. and Javaherdashti, R., *Evaluation of sessile microorganisms in pipelines and cooling towers of some Iranian industries.* Journal of materials engineering and performance, 2006. **15**(1): p. 5-8.

53. Fauque, G.D., *Ecology of sulfate-reducing bacteria*, in *Sulfate-Reducing Bacteria*1995, Springer. p. 217-241.

54. von Wolzogen Kuehr, C. and Van der Vlugt, L., *Graphitization of cast iron as an electrobiochemical process in anaerobic soils*, 1964, ARMY BIOLOGICAL LABS FREDERICK MD.

55. Videla, H., *Corrosion of Mild Steel Induced by Sulphate Reducing Bacteria--a Study of Passivity Breakdown by Biogenic Sulphides.* Biologically induced corrosion, 1985: p. 162-170.

56. Lee, W. and Characklis, W.G., *Corrosion of mild steel under anaerobic biofilm.* Corrosion, 1993. **49**(3): p. 186-199.

57. Tiller, K., *A REVIEW OF THE EUROPEAN RESEARCH EFFORT ON MICROBIAL CORROSION BETWEEN 1950 AND 1984 A.* 1950.

58. Jack, T., Rogoz, E., Bramhill, B., and Roberge, P., *The Characterization of Sulfate-Reducing Bacteria in Heavy Oil Waterflood Operations*, in *Microbiologically influenced corrosion testing*1994, ASTM International.

59. Haynie, F. and Upham, J., *Correlation between corrosion behavior of steel and atmospheric pollution data*, in *Corrosion in Natural Environments*1974, ASTM International.

60. Feliu, S. and Morcillo, M., *The prediction of atmospheric corrosion from meteorological and pollution parameters—I. Annual corrosion.* Corrosion Science, 1993. **34**(3): p. 403-414.

61. Hou, W., *ATMOSPHERIC CORROSION OF CARBON STEELS AND LOW ALLOY STEELS(Chinese).* J. Chinese Soc. of Corrosion and Protection, 1993. **13**(4): p. 291-302.

62. Morcillo, M., Simancas, J., and Feliu, S., *Long-term atmospheric corrosion in Spain: results after 13–16 years of exposure and comparison with worldwide data*, in *Atmospheric Corrosion*1995, ASTM International.

63. Wen, Y., Cai, C., Liu, X., Pei, J., Zhu, X., and Xiao, T., *Corrosion rate prediction of 3C steel under different seawater environment by using support vector regression.* Corrosion Science, 2009. **51**(2): p. 349-355.

64. Vapnik, V., *The nature of statistical learning theory Springer New York Google Scholar.* 1995.

65. Smola, A.J. and Schölkopf, B., *A tutorial on support vector regression.* Statistics and computing, 2004. **14**(3): p. 199-222.

66. Mousavifard, S., Attar, M., Ghanbari, A., and Dadgar, M., *Application of artificial neural network and adaptive neuro-fuzzy inference system to investigate corrosion rate of zirconium-based nano-ceramic layer on galvanized steel in 3.5% NaCl solution.* Journal of alloys and compounds, 2015. **639**: p. 315-324.

67. Kartalopoulos, S.V. and Kartakapoulos, S.V., *Understanding neural networks and fuzzy logic: basic concepts and applications*1997: Wiley-IEEE Press.

68. Novák, V., Perfilieva, I., and Mockor, J., *Mathematical principles of fuzzy logic*. Vol. 517. 2012: Springer Science & Business Media.

69. Jang, J.-S., *ANFIS: adaptive-network-based fuzzy inference system.* IEEE transactions on systems, man, and cybernetics, 1993. **23**(3): p. 665-685.

70. Pintos, S., Queipo, N.V., de Rincón, O.T., Rincón, A., and Morcillo, M., *Artificial neural network modeling of atmospheric corrosion in the MICAT project.* Corrosion Science, 2000. **42**(1): p. 35-52.

71. Parthiban, T., Ravi, R., Parthiban, G., Srinivasan, S., Ramakrishnan, K., and Raghavan, M., *Neural network analysis for corrosion of steel in concrete.* Corrosion Science, 2005. **47**(7): p. 1625-1642.

72. Cai, J., Cottis, R., and Lyon, S., *Phenomenological modelling of atmospheric corrosion using an artificial neural network.* Corrosion Science, 1999. **41**(10): p. 2001-2030.

73. Morcous, G. and Lounis, Z., *Prediction of Onset of Corrosion in Concrete Bridge Decks Using Neural Networks and Case-Based Reasoning.* Computer-Aided Civil and Infrastructure Engineering, 2005. **20**(2): p. 108-117.

74. Hertz, J., Krogh, A., and Palmer, R.G., *Introduction to the theory of neural computation*. Vol. 1. 1991: Basic Books.

75. Helliwell, I., Turega, M., and Cottis, R., *Neural networks for corrosion data reduction*, 1996, NACE International, Houston, TX (United States).

76. Cottis, R., Qing, L., Owen, G., Gartland, S., Helliwell, I., and Turega, M., *Neural network methods for corrosion data reduction.* Materials & Design, 1999. **20**(4): p. 169-178.

77. Fang, S., Wang, M., Qi, W., and Zheng, F., *Hybrid genetic algorithms and support vector regression in forecasting atmospheric corrosion of metallic materials.* Computational Materials Science, 2008. **44**(2): p. 647-655.

78. Jančíková, Z., Roubíček, V., and Juchelková, D., *Rabljenje metode umjetne inteligencije za predmnijevanje mehaničkih svojstava čelika.* Metalurgija, 2008. **47**(4): p. 339-342.

79. Jančíková, Z., Zimný, O., and Koštial, P., *Prediction of metal corrosion by neural networks.* Metalurgija, 2013. **52**(3): p. 379-381.

80. Rosen, E. and Silverman, D., *Corrosion prediction from polarization scans using an artificial neural network integrated with an expert system.* Corrosion, 1992. **48**(9): p. 734-745.

81. Trasatti, S. and Mazza, F., *Crevice corrosion: a neural network approach.* British Corrosion Journal, 1996. **31**(2): p. 105-112.

82. Smets, H. and Bogaerts, W., *SCC analysis of austenitic stainless steels in chloride-bearing water by neural network techniques.* Corrosion, 1992. **48**(8): p. 618-623.

83. Graupe, D., *Identification of systems*, 1972, Van Nostrand Reinhold Company.

84. Natke, H.G., *Application of system identification in engineering*. Vol. 296. 2014: Springer.

85. Specht, D.F., *A general regression neural network.* IEEE transactions on neural networks, 1991. **2**(6): p. 568-576.

86. Tao, N., Wang, Z., Tong, W., Sui, M., Lu, J., and Lu, K., *An investigation of surface nanocrystallization mechanism in Fe induced by surface mechanical attrition treatment.* Acta materialia, 2002. **50**(18): p. 4603-4616.

87. Liu, G., Wang, S., Lou, X., Lu, J., and Lu, K., *Low carbon steel with nanostructured surface layer induced by high-energy shot peening.* Scripta Materialia, 2001. **44**(8): p. 1791-1795.

88. Balusamy, T., Kumar, S., and Narayanan, T.S., *Effect of surface nanocrystallization on the corrosion behaviour of AISI 409 stainless steel.* Corrosion Science, 2010. **52**(11): p. 3826-3834.

89. Chen, A., Li, Y., Zhang, J., Pan, D., and Lu, J., *The influence of interface structure on nanocrystalline deformation of a layered and nanostructured steel.* Materials & Design, 2013. **47**: p. 316-322.

90. Fu, T., Zhan, Z., Zhang, L., Yang, Y., Liu, Z., Liu, J., Li, L., and Yu, X., *Effect of surface mechanical attrition treatment on corrosion resistance of commercial pure titanium.* Surface and Coatings Technology, 2015. **280**: p. 129-135.

91. Liu, Y., Jin, B., Li, D.-J., Zeng, X.-Q., and Lu, J., *Wear behavior of nanocrystalline structured magnesium alloy induced by surface mechanical attrition treatment.* Surface and Coatings Technology, 2015. **261**: p. 219-226.

92. Multigner, M., Frutos, E., González-Carrasco, J., Jiménez, J., Marín, P., and Ibáñez, J., *Influence of the sandblasting on the subsurface microstructure of 316LVM stainless steel: Implications on the magnetic and mechanical properties.* Materials Science and Engineering: C, 2009. **29**(4): p. 1357-1360.

93. Azar, V., Hashemi, B., and Yazdi, M.R., *The effect of shot peening on fatigue and corrosion behavior of 316L stainless steel in Ringer's solution.* Surface and Coatings Technology, 2010. **204**(21-22): p. 3546-3551.

94. Peyre, P., Scherpereel, X., Berthe, L., Carboni, C., Fabbro, R., Beranger, G., and Lemaitre, C., *Surface modifications induced in 316L steel by laser peening and shot-peening. Influence on pitting corrosion resistance.* Materials Science and Engineering: A, 2000. **280**(2): p. 294-302.

95. Liu, G., Lu, J., and Lu, K., *Surface nanocrystallization of 316L stainless steel induced by ultrasonic shot peening.* Materials Science and Engineering: A, 2000. **286**(1): p. 91-95.

96. Dai, K., Villegas, J., Stone, Z., and Shaw, L., *Finite element modeling of the surface roughness of 5052 Al alloy subjected to a surface severe plastic deformation process.* Acta Materialia, 2004. **52**(20): p. 5771-5782.

97. Lu, K. and Lu, J., *Nanostructured surface layer on metallic materials induced by surface mechanical attrition treatment.* Materials Science and Engineering: A, 2004. **375**: p. 38-45.

98. Astaraee, A.H., Miresmaeili, R., Bagherifard, S., Guagliano, M., and Aliofkhazraei, M., *Incorporating the principles of shot peening for a better understanding of surface mechanical attrition treatment (SMAT) by simulations and experiments*. Materials & Design, 2017. **116**: p. 365-373.

99. Bagherifard, S., Slawik, S., Fernández-Pariente, I., Pauly, C., Mücklich, F., and Guagliano, M., *Nanoscale surface modification of AISI 316L stainless steel by severe shot peening.* Materials & Design, 2016. **102**: p. 68-77.

100. Multigner, M., Ferreira-Barragáns, S., Frutos, E., Jaafar, M., Ibáñez, J., Marín, P., Pérez-Prado, M., González-Doncel, G., Asenjo, A., and González-Carrasco, J., *Superficial severe plastic deformation of 316 LVM stainless steel through grit blasting: Effects on its microstructure and subsurface mechanical properties.* Surface and Coatings Technology, 2010. **205**(7): p. 1830-1837.

101. Rudawska, A., Danczak, I., Müller, M., and Valasek, P., *The effect of sandblasting on surface properties for adhesion.* International Journal of Adhesion and Adhesives, 2016. **70**: p. 176-190.

102. Geng, S., Sun, J., and Guo, L., *Effect of sandblasting and subsequent acid pickling and passivation on the microstructure and corrosion behavior of 316L stainless steel.* Materials & Design, 2015. **88**: p. 1-7.

103. Pour-Ali, S., Kiani-Rashid, A.-R., and Babakhani, A., *Surface nanocrystallization and gradient microstructural evolutions in the surface layers of 321 stainless steel alloy treated via severe shot peening.* Vacuum, 2017. **144**: p. 152-159.

104. Pour-Ali, S., Kiani-Rashid, A.-R., Babakhani, A., Virtanen, S., and Allieta, M., *Correlation between the surface coverage of severe shot peening and surface*

microstructural evolutions in AISI 321: A TEM, FE-SEM and GI-XRD study. Surface and Coatings Technology, 2018. **334**: p. 461-470.

105. Jayalakshmi, M., Huilgol, P., Bhat, B.R., and Bhat, K.U., *Microstructural characterization of low temperature plasma-nitrided 316L stainless steel surface with prior severe shot peening.* Materials & Design, 2016. **108**: p. 448-454.

106. Mordyuk, B., Karasevskaya, O., Prokopenko, G., and Khripta, N., *Ultrafine-grained textured surface layer on Zr–1% Nb alloy produced by ultrasonic impact peening for enhanced corrosion resistance.* Surface and Coatings Technology, 2012. **210**: p. 54-61.

107. Benafia, S., Retraint, D., Brou, S.Y., Panicaud, B., and Poussard, J.G., *Influence of Surface Mechanical Attrition Treatment on the oxidation behaviour of 316L stainless steel.* Corrosion Science, 2018.

108. Chen, T., John, H., Xu, J., Lu, Q., Hawk, J., and Liu, X., *Influence of surface modifications on pitting corrosion behavior of nickel-base alloy 718. Part 1: Effect of machine hammer peening.* Corrosion Science, 2013. **77**: p. 230-245.

109. Yin, Z., Yang, X., Ma, X., Moering, J., Yang, J., Gong, Y., Zhu, Y., and Zhu, X., *Strength and ductility of gradient structured copper obtained by surface mechanical attrition treatment.* Materials & Design, 2016. **105**: p. 89-95.

110. An, Y.-l., Du, H.-y., Wei, Y.-h., Wang, N., Hou, L.-f., and Lin, W.-m., *Interfacial structure and mechanical properties of surface iron–nickel alloying layer in pure iron fabricated by surface mechanical attrition alloy treatment.* Materials & Design, 2013. **46**: p. 627-633.

111. Hassani, S., Raeissi, K., Azzi, M., Li, D., Golozar, M., and Szpunar, J., *Improving the corrosion and tribocorrosion resistance of Ni–Co nanocrystalline coatings in NaOH solution.* Corrosion Science, 2009. **51**(10): p. 2371-2379.

112. Hou, J., Peng, Q., Lu, Z., Shoji, T., Wang, J., Han, E.-H., and Ke, W., *Effects of cold working degrees on grain boundary characters and strain concentration at grain boundaries in Alloy 600.* Corrosion Science, 2011. **53**(3): p. 1137-1142.

113. Hamdy, A.S., El-Shenawy, E., and El-Bitar, T., *Electrochemical impedance spectroscopy study of the corrosion behavior of some niobium bearing stainless steels in 3.5% NaCl.* International Journal of Electrochemical Science, 2006. **1**(4): p. 171-80.

114. Wang, T., Yu, J., and Dong, B., *Surface nanocrystallization induced by shot peening and its effect on corrosion resistance of 1Cr18Ni9Ti stainless steel.* Surface and Coatings Technology, 2006. **200**(16-17): p. 4777-4781.

115. Hamu, G.B., Eliezer, D., and Wagner, L., *The relation between severe plastic deformation microstructure and corrosion behavior of AZ31 magnesium alloy.* Journal of alloys and compounds, 2009. **468**(1-2): p. 222-229.

116. Lee, H.-s., Kim, D.-s., Jung, J.-s., Pyoun, Y.-s., and Shin, K., *Influence of peening on the corrosion properties of AISI 304 stainless steel.* Corrosion science, 2009. **51**(12): p. 2826-2830.

117. Mordyuk, B., Prokopenko, G., Vasylyev, M., and Iefimov, M., *Effect of structure evolution induced by ultrasonic peening on the corrosion behavior of AISI-321 stainless steel.* Materials Science and Engineering: A, 2007. **458**(1-2): p. 253-261.

118. Torbati-Sarraf, H. and Poursaee, A., *Corrosion of coupled steels with different microstructures in concrete environment.* Construction and Building Materials, 2018. **167**: p. 680-687.

119. Chintapalli, R.K., Rodriguez, A.M., Marro, F.G., and Anglada, M., *Effect of sandblasting and residual stress on strength of zirconia for restorative dentistry applications.* Journal of the mechanical behavior of biomedical materials, 2014. **29**: p. 126-137.

120. Chintapalli, R.K., Marro, F.G., Jimenez-Pique, E., and Anglada, M., *Phase transformation and subsurface damage in 3Y-TZP after sandblasting.* Dental Materials, 2013. **29**(5): p. 566-572.

121. Raykowski, A., Hader, M., Maragno, B., and Spelt, J., *Blast cleaning of gas turbine components: deposit removal and substrate deformation.* Wear, 2001. **249**(1): p. 126-131.

122. Yuan, L., Chen, X., Maganty, S., Cho, J., Ke, C., and Zhou, G., *Enhancing the oxidation resistance of copper by using sandblasted copper surfaces.* Applied Surface Science, 2015. **357**: p. 2160-2168.

123. Wang, X. and Li, D., *Mechanical and electrochemical behavior of nanocrystalline surface of 304 stainless steel.* Electrochimica Acta, 2002. **47**(24): p. 3939-3947.

124. Hou, J., Fu, X., and Chung, D., *Improving both bond strength and corrosion resistance of steel rebar in concrete by water immersion or sand blasting of rebar*. Cement and concrete research, 1997. **27**(5): p. 679-684.

125. ASTM, *ASTM D2974-87, standard test method for moisture,ash, and organic matter of peat and other organic soils.*, 2000, ASTM International.

126. EPA, *Method 9045D: Soil and waste pH.* 2004.

127. EPA, *Method 120.1: Conductance (Specific Conductance, umhos at 25°C) by conductivity meter.* 1982.

128. Hautman, D.P. and Munch, D.J., *Method 300.1 Determination of inorganic anions in drinking water by ion chromatography.* EPA: Ohio, 1997.

129. EPA, *Method 9060: Total Organic Carbon (TOC) in soil*. 2010.

130. ASTM, *G5-94: Standard Reference Test Method for Making Potentiostatic and Potentiodynamic Anodic Polarization Measurements*, 2004, ASTM.

131. *ImageJ*: National Institutes of Health, http://rsbweb.nih.gov/ij/.

132. Poursaee, A., *Potentiostatic transient technique, a simple approach to estimate the corrosion current density and Stern–Geary constant of reinforcing steel in concrete.* Cement and Concrete Research, 2010. **40**: p. 1451–1458.

133. Oldfield, J.W., *Electrochemical theory of galvanic corrosion*, in *Galvanic Corrosion*1988, ASTM International.

134. Railsback, S.F. and Grimm, V., *Agent-based and individual-based modeling: a practical introduction*2011: Princeton university press.

135. Videla, H.A., *Manual of biocorrosion*1996: CRC Press.